Electronic Supplementary Material (ESI) for Dalton Transactions.

Supporting Information For:

Naphthalimide Functionalized Metal-Organic Framework for Rapid and Nanomolar Level Detection of Hydrazine and Anti-hypertensive Drug Nicardipine

Sk Sakir Hossain, [a] *Dirk Volkmer,* [b] *and Shyam Biswas* [a]*

[a] Department of Chemistry, Indian Institute of Technology Guwahati, 781039, Assam, India.

[b] University of Augsburg, Institute of Physics, Chair of Solid State and Materials Chemistry, Universitaetsstrasse 1, 86159 Augsburg, Germany.

*Corresponding author. Tel: 91-3612583309

E-mail address: sbiswas@iitg.ac.in

Materials and Characterization Methods:

All of the chemicals were purchased from commercial suppliers and used directly. The 2-(6-bromo-1,3-dioxo-1H-benzo[de]isoquinolin-2(3H)-yl) terephthalic acid linker (H_2L) was prepared according to the below mentioned procedure. The Attenuated Total Reflectance Infrared (ATR-IR) spectra were recorded using PerkinElmer UATR Two at the ambient condition in the region 400-4000 cm^{-1}. The notations used for characterization of the bands are broad (br), strong (s), very strong (vs), medium (m), weak (w) and shoulder (sh). Fluorescence sensing studies were performed with a HORIBA JOBIN YVON Fluoromax-4 spectrofluorometer. A Bruker Avance III 600 NMR spectrometer was used for recording ^{1}H and ^{13}C NMR spectra at 500 MHz. Thermogravimetric analysis (TGA) was carried out with a Netzsch STA-409CD thermal analyzer in the temperature range of 30-700 °C in an O_2 atmosphere at the heating rate of 4 °C min^{-1}. PXRD data were collected by using Rigaku Smartlab X-ray diffractometer with Cu-Kα radiation, 40 kV of operating voltage and 125 mA of operating current. N_2 sorption isotherms were recorded by using Quantachrome Quadrasorb evo volumetric gas adsorption equipment at −196 °C. Before the sorption analysis, the degassing of the compound was carried out at 100 °C under a high vacuum for 24 h. Gemini 500 was utilized for Energy Dispersive X-rays spectrometer (EDX) for elemental characterization. FE-SEM images were captured with a Zeiss (SIGMA 300) scanning electron microscope. Pawley refinement was carried out using Materials Studio software.[1]

Preparation MOF (1') Suspension for Fluorescence Experiments:

We chose water as a sensing medium for the fluorometric sensing of hydrazine with the synthesised MOF (**1'**). The MOF suspension was first prepared for sensing. 4 mg of 1' was taken in a glass vial, and 4 mL of distilled water was added. The vial was sonicated for 30 minutes. Subsequently, the prepared suspension vial was left undisturbed at room temperature overnight to ensure its stability. For the fluorescence experiment, 300 µL of the aforementioned stable suspension was carefully transferred into a quartz container, containing 3 mL of distilled water. Fluorescence measurements were then conducted across the wavelength range of 360-610 nm, with excitation of the suspension at 340 nm for hydrazine sensing. For nicardipine sensing the fluorescence data were recorded within the range of 490-630 nm and rest were similar to previous.

Fluorometric Detection of Ranitidine in Human Blood Serum Sample:

From the right arm vein of a healthy human with blood group A^+, 10 mL of blood sample was collected. The sample was centrifuged at 10,000 rpm for 15 min to obtain blood plasma, from which the light-yellow blood serum was collected and stored in a Falcon tube at -20 °C. To conduct fluorescence detection experiments, varying concentrations of ranitidine were added to different aliquots of the human blood serum sample containing a MOF suspended in HEPES buffer (pH = 7.4).

Fluorometric Detection of Ranitidine in Human Urine Sample:

A 10 mL urine sample was collected from a healthy individual and treated with 500 mL of HNO_3 to eliminate any interfering living organisms. The sample was then centrifuged at 8000 rpm for 10 min, and the supernatant was used for the experiments. To conduct fluorescence

experiments, various amounts of ranitidine were added to the urine samples containing a HEPES buffer suspension of the probe.

Synthetic Procedure for 2-(6-Bromo-1, 3-Dioxo-1H-Benzo[de]Isoquinolin-2(3H)-yl) Terephthalic Acid Linker (H_2L):

In a 50 mL round-bottom flask 181 mg (1 mmol) of 2-amino terephthalic acid is taken and dissolved in 5 mL of anhydrous MeOH. Then, 10 drops of trimethylamine (Et3N) are added to the reaction mixture at 0°C under stirring condition. A suspension of 275 mg 4-bromo-1, 8-naphthalic anhydride in 10 mL of anhydrous MeOH is added to the previous reaction mixture dropwise under stirring condition. After that, the reaction mixture is refluxed for 24 hours at N2 atmosphere. After the completion of the reaction the reaction mixture is allowed to cool to room temperature and poured to 50 mL ice cold distilled water. The reaction mixture is acidified with conc. HCl and then precipitation took place. The product is collected by vacuum filtration and washed several times with distilled water. Finally, the product is dried in a hot air oven at 80 °C. The ^{1}H NMR and ^{13}C NMR data were recorded of the linker. The ^{1}H NMR and ^{13}C NMR data are shown in Figure 1a and 1b respectively.

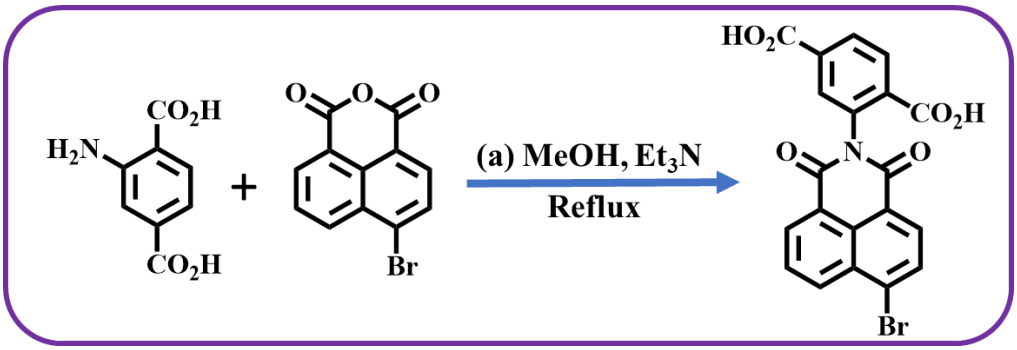

Scheme 1. Reaction scheme for the synthesis of H_2L linker.

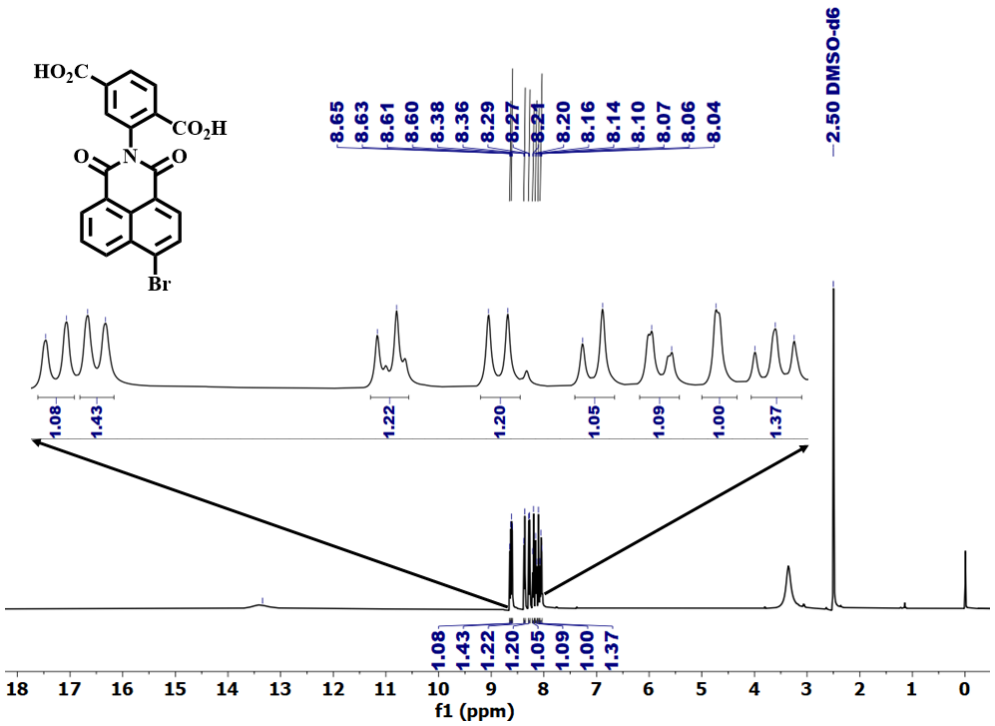

Figure S1. ^{1}H NMR spectrum (500 MHz, DMSO-d_6) of H_2L linker.

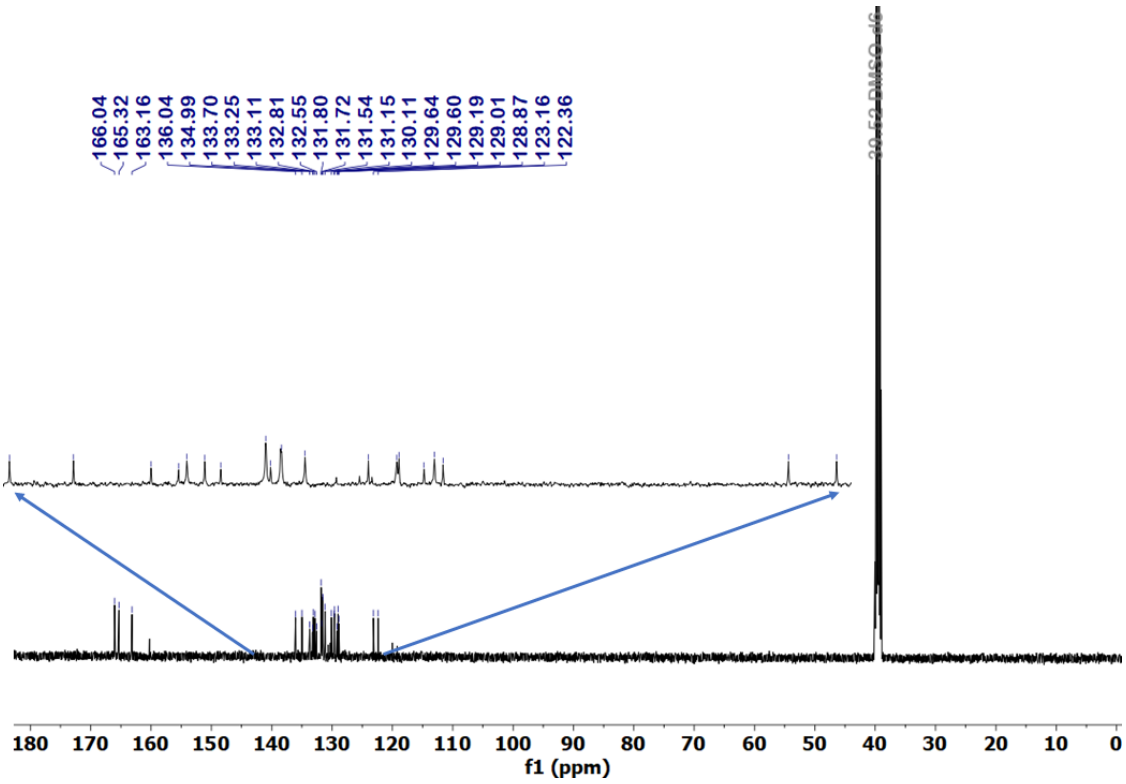

Figure S2. ^{13}C NMR spectrum (125 MHz, DMSO-d_6) of H_2L linker.

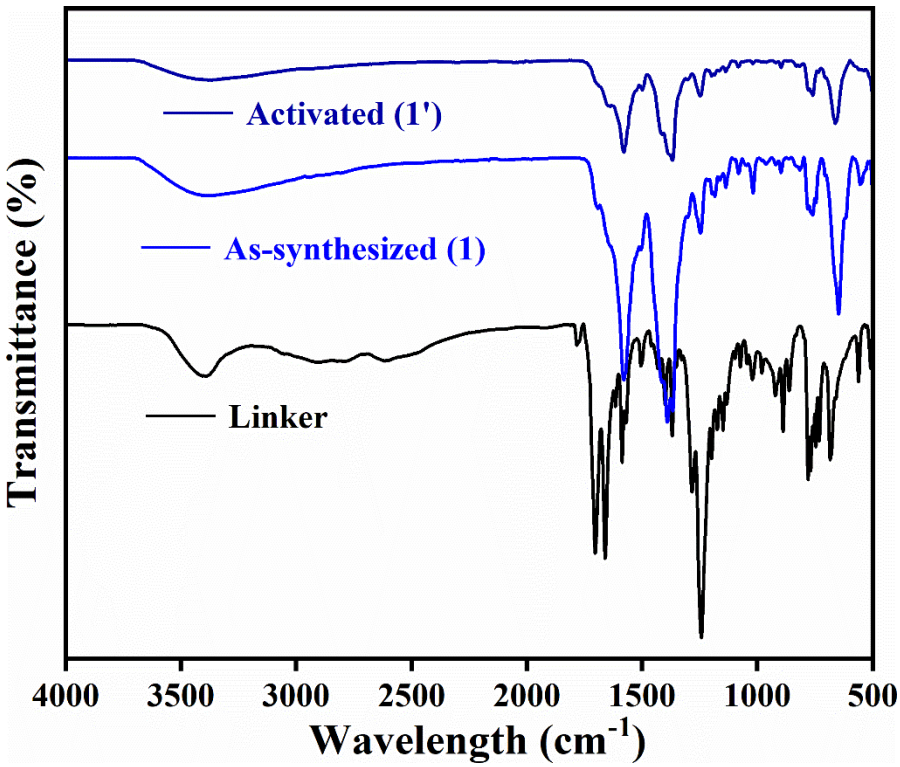

Figure S3. ATR-IR spectra of H_2L linker, **1** and **1'**.

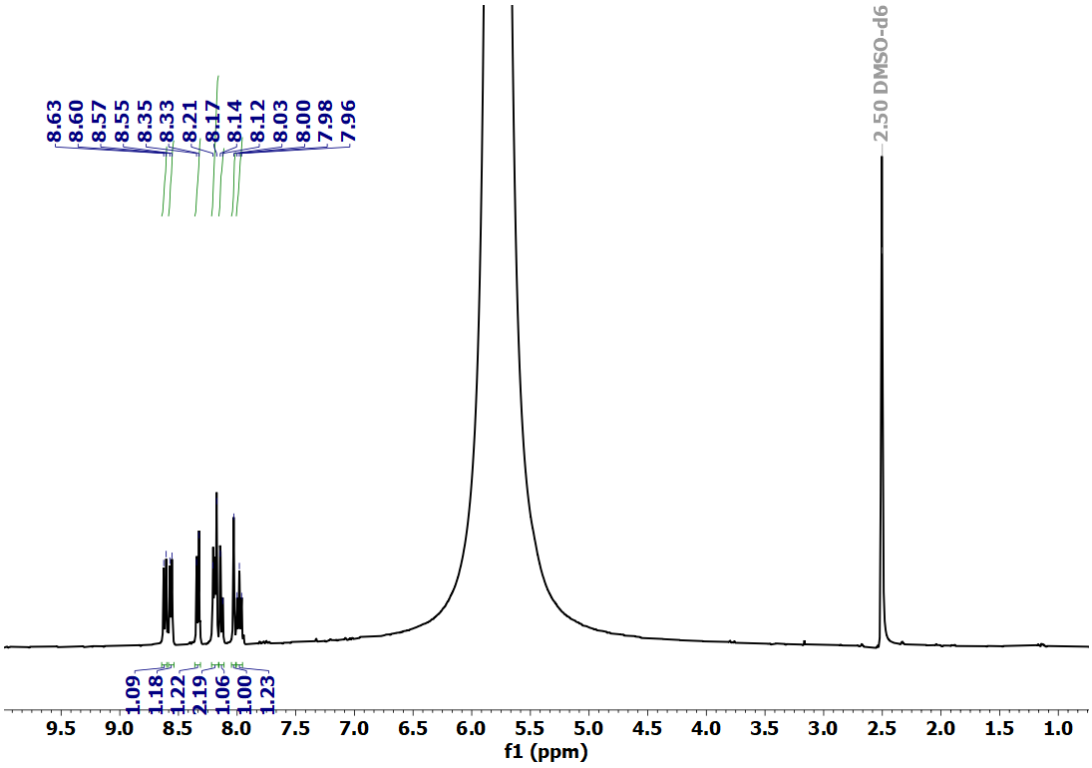

Figure S4. ^{1}H NMR spectrum of digested **1'** (digested using 100 µL of 40% HF in 500 µL of DMSO-d_6).

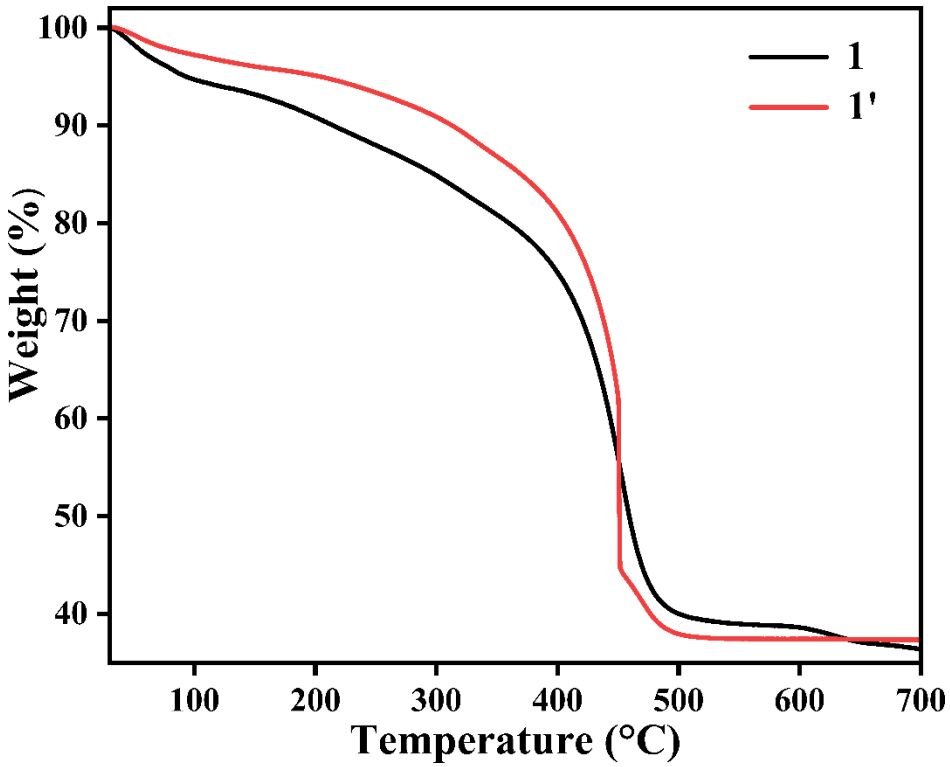

Figure S5. TGA curves of **1** and **1'** recorded under O_2 atmosphere in the temperature range of 30-700 °C with a heating rate 4 °C/min.

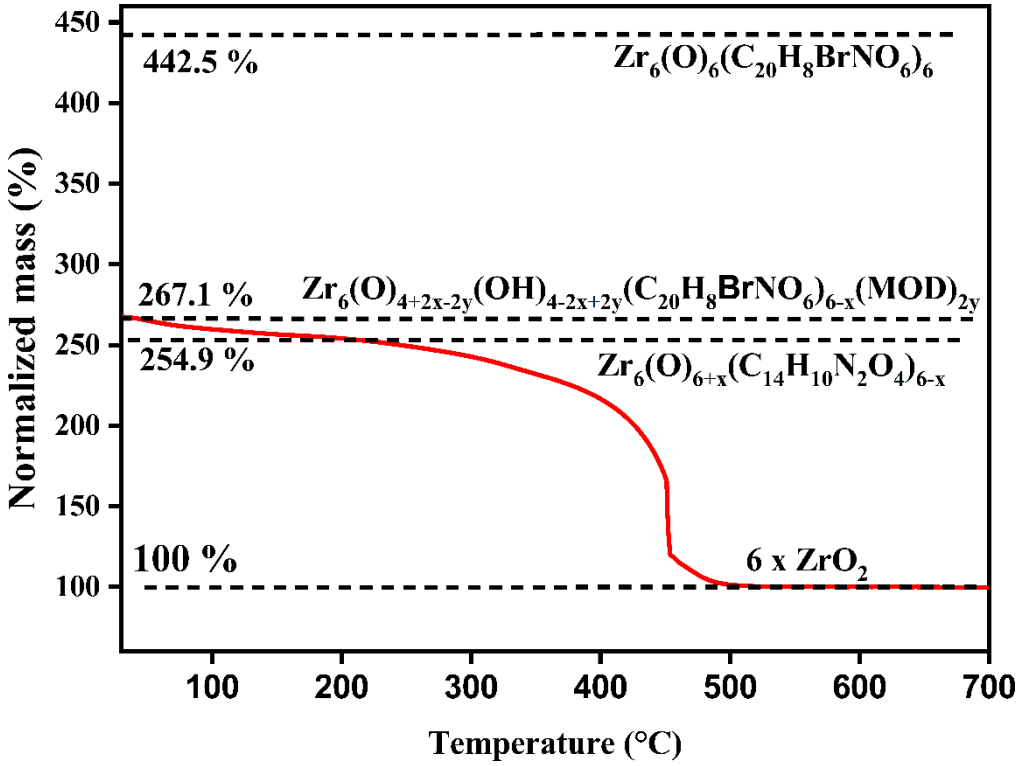

Figure S6. Calculation of missing ligand defects from the TG curve of activated **1'**. The vertical dashed line pinpoints $T_{Plat.}$, the temperature at which the plateau ($W_{Exp.\ Plat.}$) is reached. The horizontal dashed lines pinpoint the relevant TGA plateaus.

Calculation of Linker Defects for 1' from TGA Data:

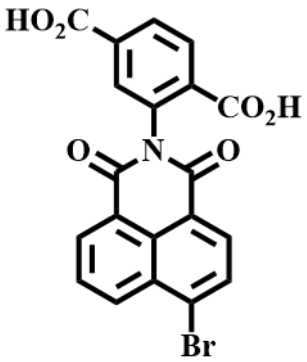

2-(6-bromo-1,3-dioxo-1H-benzo[de]isoquinolin-2(3H)-yl)terephthalic acid

Formula of MOF = $[Zr_6(O)_4(OH)_4(C_{10}H_{20}BrNO_6)_6]$

Molecular weight = 3307.3 g/mol

- The dehydroxylated and modulator free formula of MOF is $[Zr_6(O)_6(C_{10}H_{20}BrNO_6)_6]$ (ideal),
- Molecular Weight = 3271.3 g/mol
- The dehydroxylated and modulator free formula of MOF is $[Zr_6(O)_{6+x}(C_{10}H_{20}BrNO_6)_{6-x}]$ (experimental), Molecular Weight = 3271.3 g/mol (x = number of linker defect).
- From TGA data, after final weight loss step, the remaining mass is due to 6 moles of ZrO_2 i.e. 6 × 123.2 = 739.3 g/mol.
- The ideal weight of $[Zr_6(O)_6(C_{10}H_{20}BrNO_6)_6]$ is 4.42 times of 6 moles of ZrO_2.
- The remaining flat mass obtained at the last mass on TGA curve was normalized to 100%.
- The ideal normalized mass percentage for $[Zr_6(O)_6(C_{10}H_{20}BrNO_6)_6]$ is 442.4 %.
- The experimental normalized mass percentage of $[Zr_6(O)_{6+x}(C_{10}H_{20}BrNO_6)_{6-x}]$ from TGA is 254.9%.
- $x = 6 – (W_{wt.\ Plat} - W_{end}/Wt.PL._{Theo})$.

where

- $W_{wt.\ Plat}$ is the (normalized) weight of the sample at the second TGA plateau.
- W_{end} is 100 %
- $Wt.PL._{Theo} = (W_{wt.\ ideal\ Plat.} – W_{end})/NL_{ideal}$
- NL_{ideal} = number of linkers per unit formula ideally (6)
- $Wt.PL._{Theo} = ((442.4-100)/6) = 57.0$ %
- $x = 6 - ((254.9 – 100)/57) = 6 – 2.71 = 3.$
- Number of linker defect per unit formula is 3.

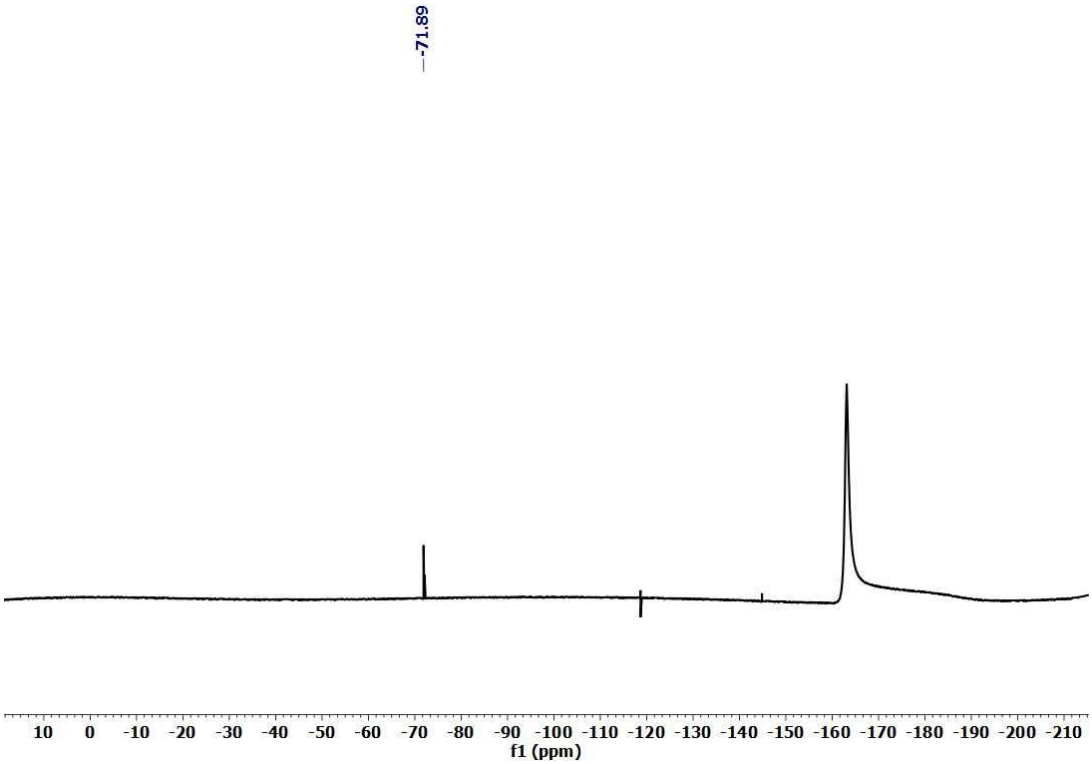

Figure S7. ^{19}F NMR spectrum of digested **1'** in DMSO-d_6 with 40% HF.

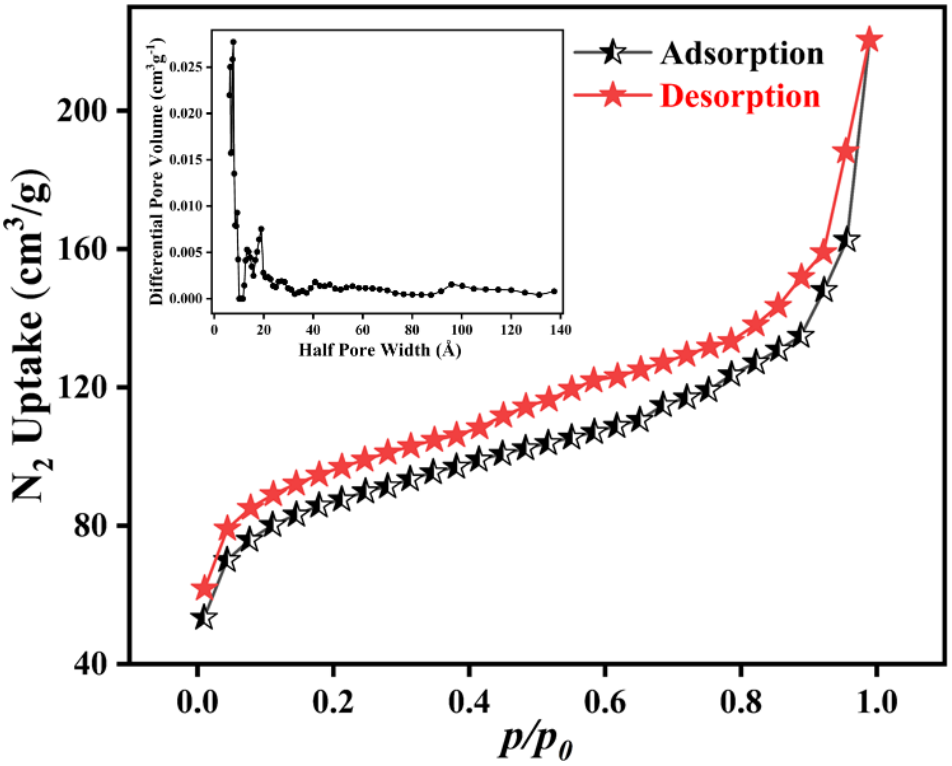

Figure S8. N_2 sorption isotherms of **1'** measured at -196 °C and density functional theory pore-size distribution of compound **1'** (shown in inset).

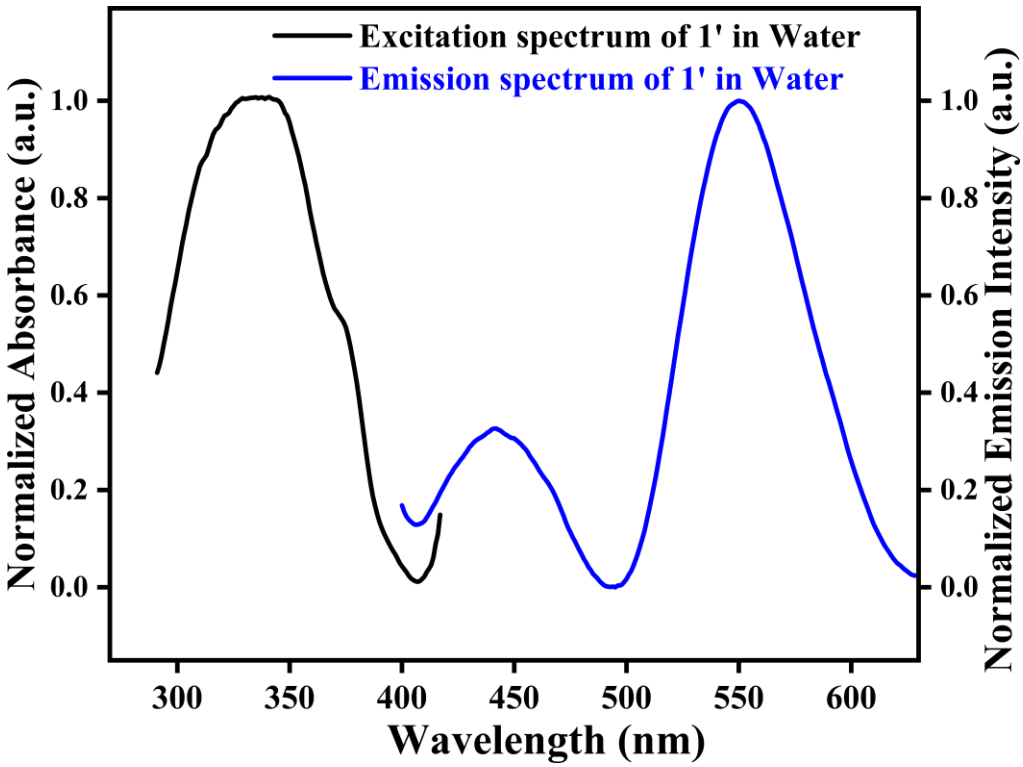

Figure S9. Fluorescence excitation and emission spectra of **1'** in water.

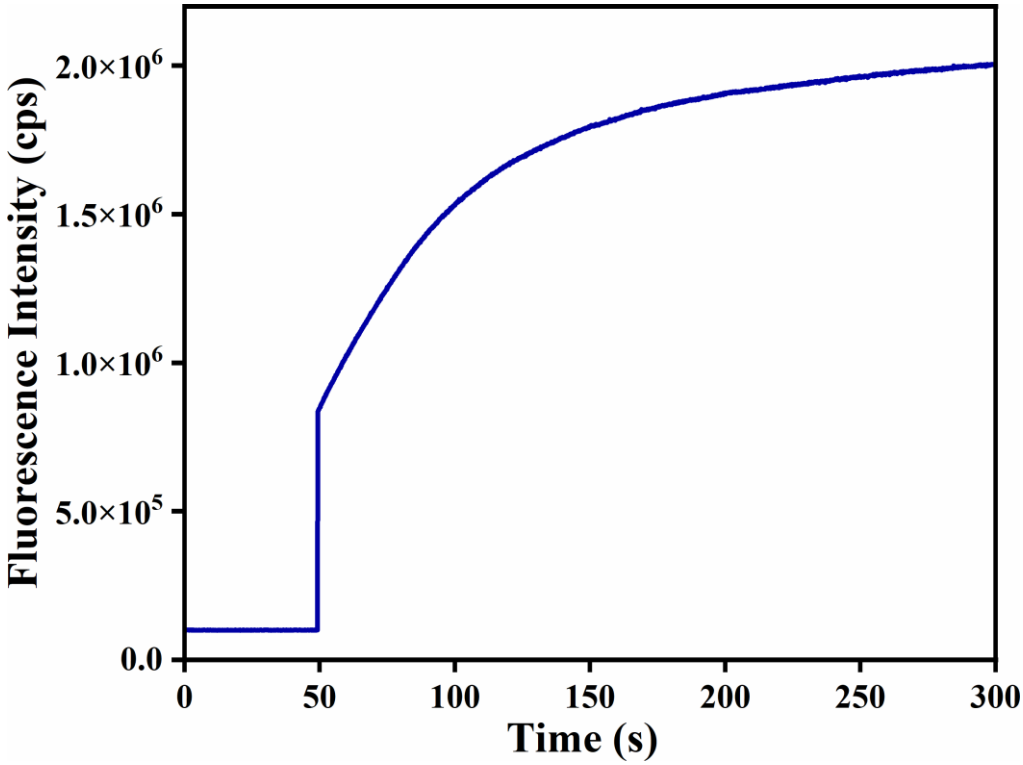

Figure S10. Fluorescence kinetic experiment for hydrazine sensing.

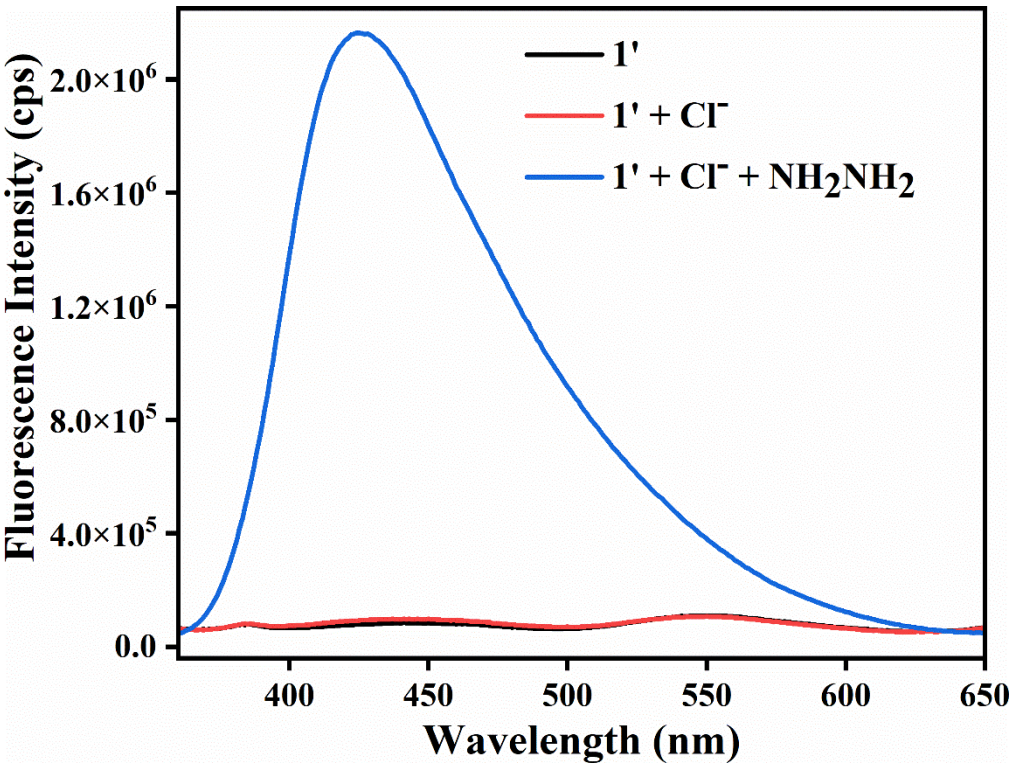

Figure S11. The fluorometric turn-on response of **1'** towards NH_2NH_2 (300 µL, 10 mM) in the presence of Cl^- (300 µL, 10 mM).

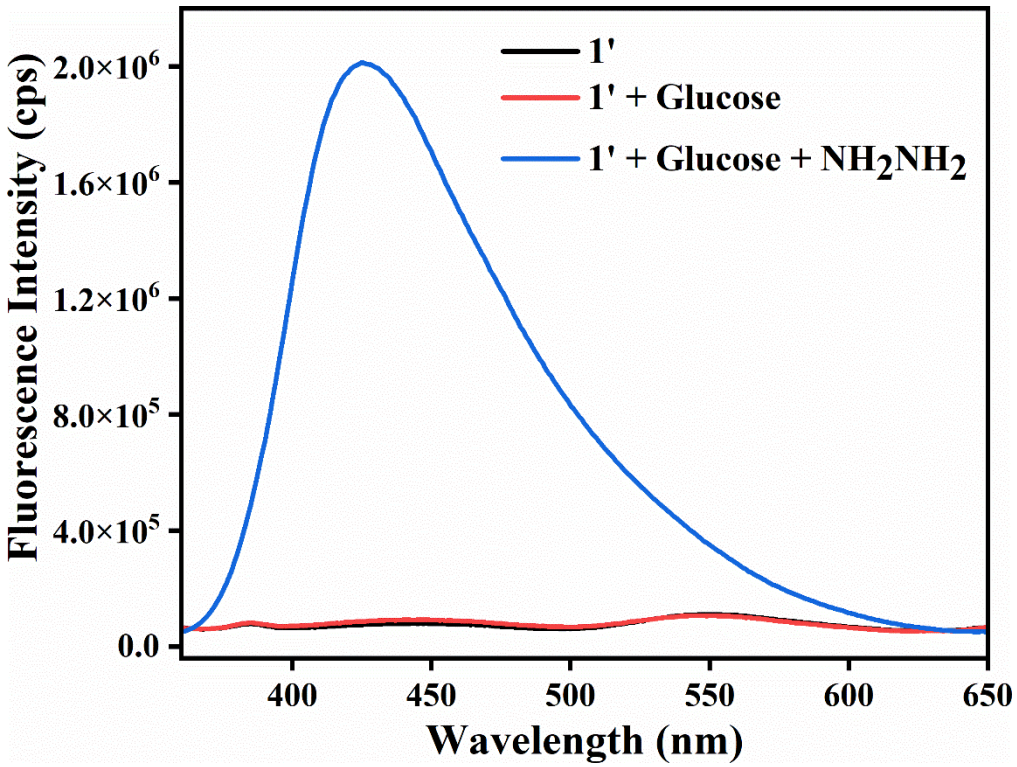

Figure S12. The fluorometric turn-on response of **1'** towards NH_2NH_2 (300 µL, 10 mM) in the presence of Glucose (300 µL, 10 mM).

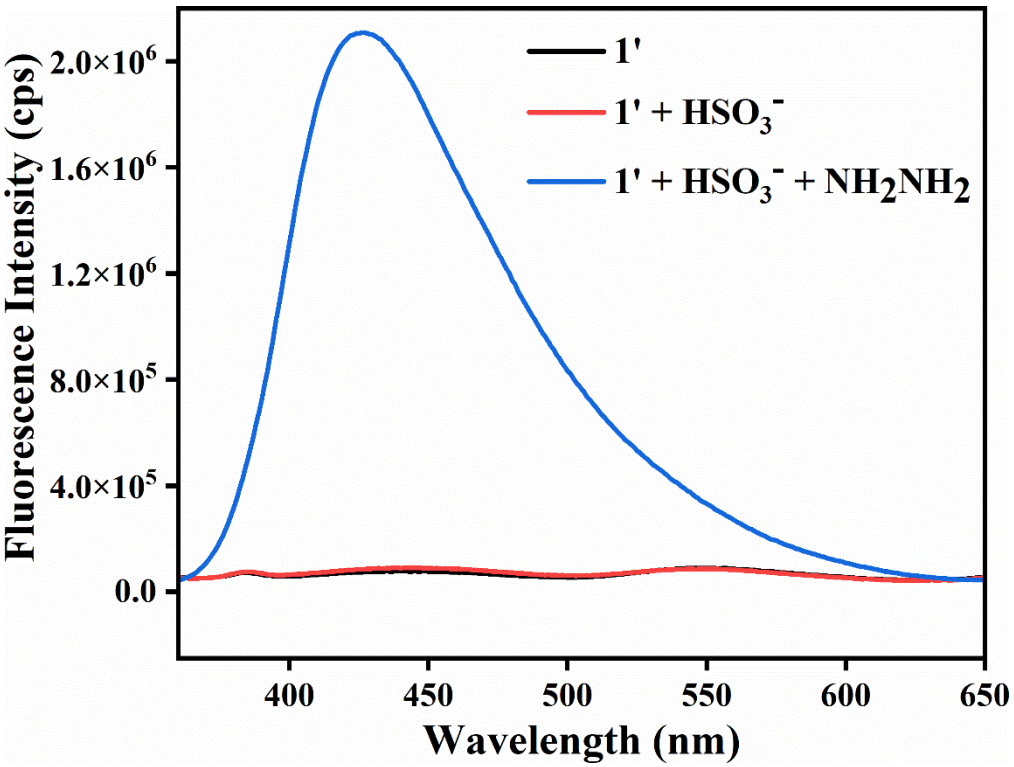

Figure S13. The fluorometric turn-on response of **1'** towards NH_2NH_2 (300 µL, 10 mM) in the presence of HSO_3^- (300 µL, 10 mM).

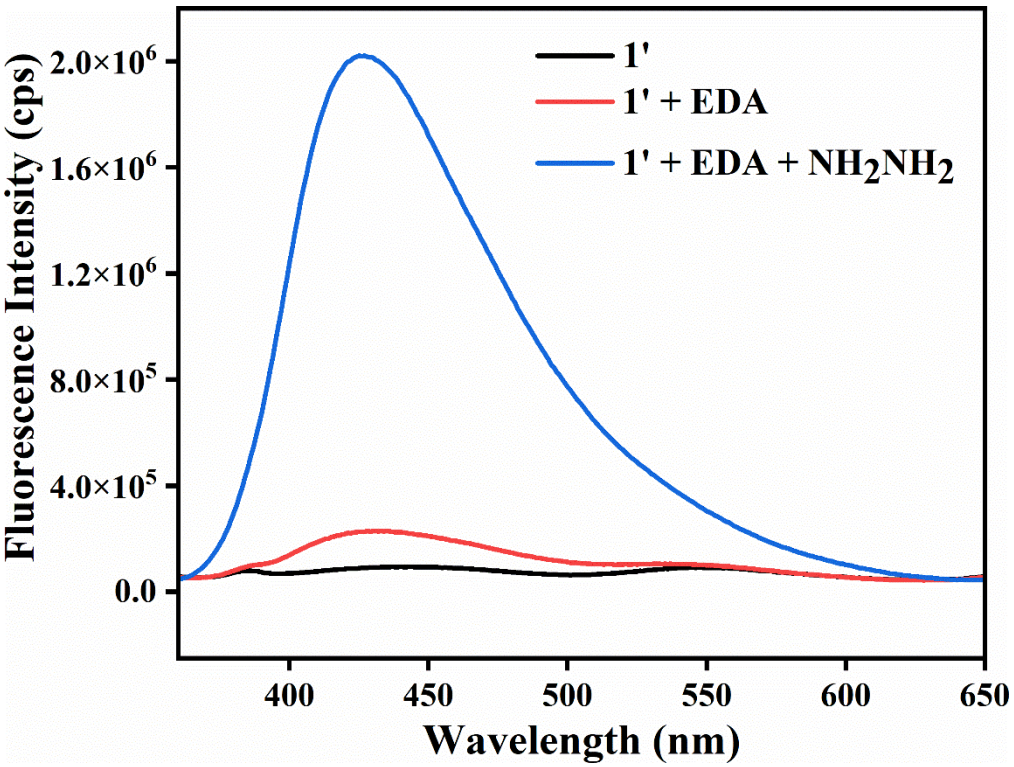

Figure S14. The fluorometric turn-on response of **1'** towards NH_2NH_2 (300 µL, 10 mM) in the presence of ethylenediamine (300 µL, 10 mM).

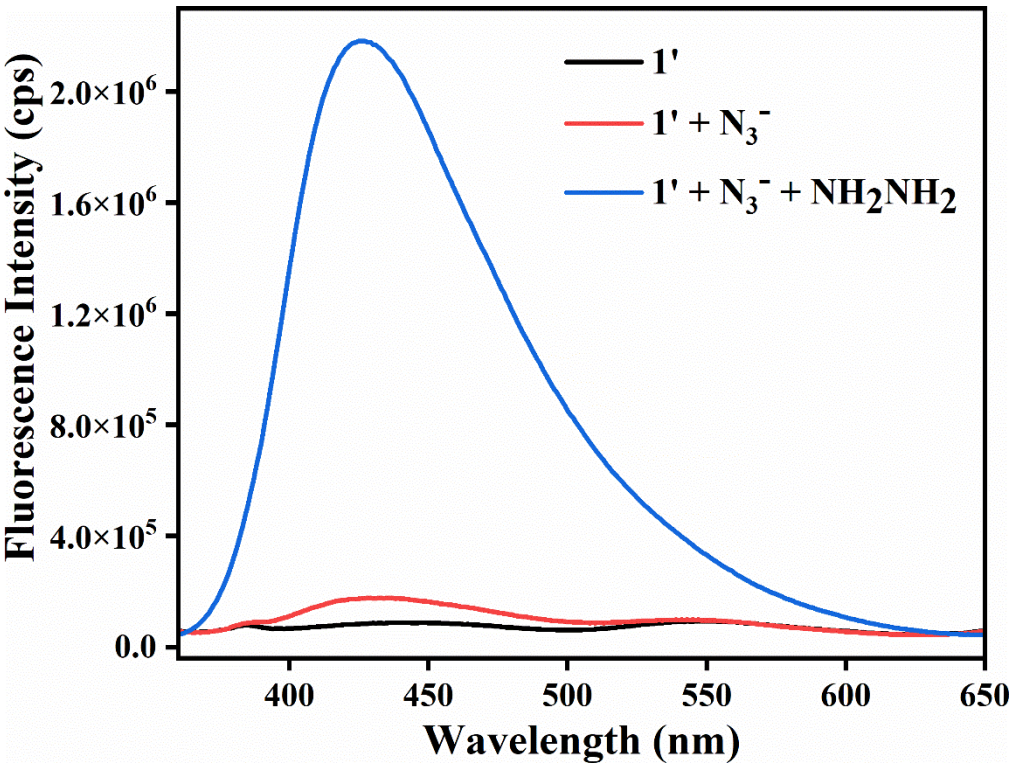

Figure S15. The fluorometric turn-on response of **1'** towards NH_2NH_2 (300 µL, 10 mM) in the presence of N_3^- (300 µL, 10 mM).

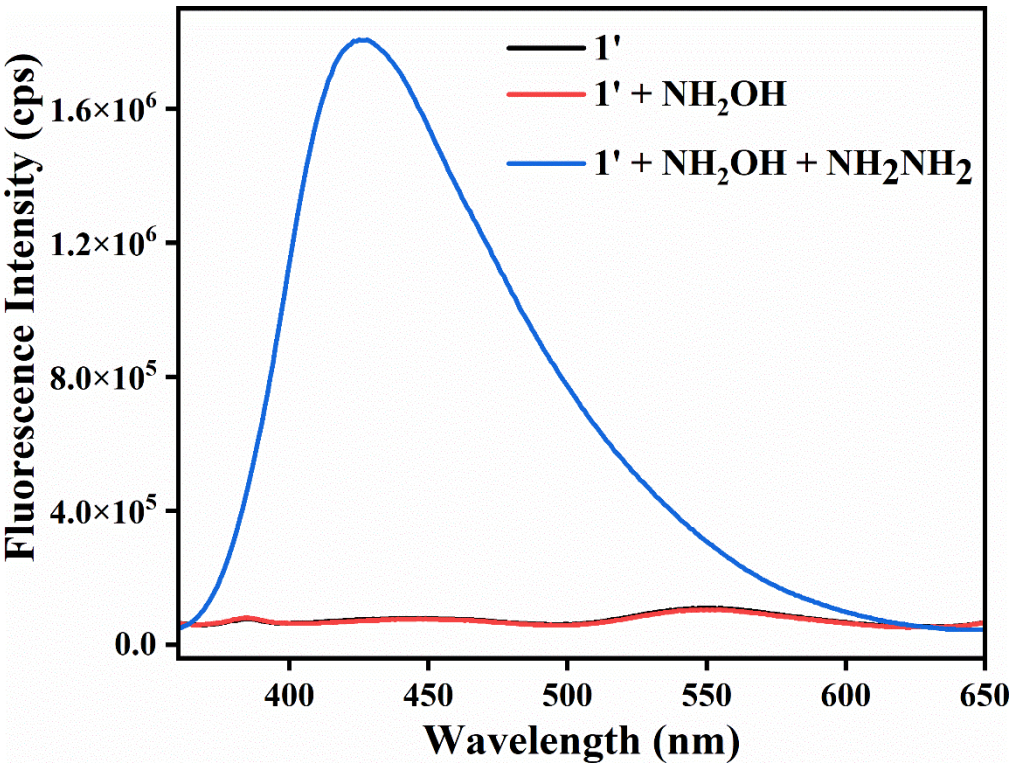

Figure S16. The fluorometric turn-on response of **1'** towards NH_2NH_2 (300 µL, 10 mM) in the presence of NH_2OH (300 µL, 10 mM).

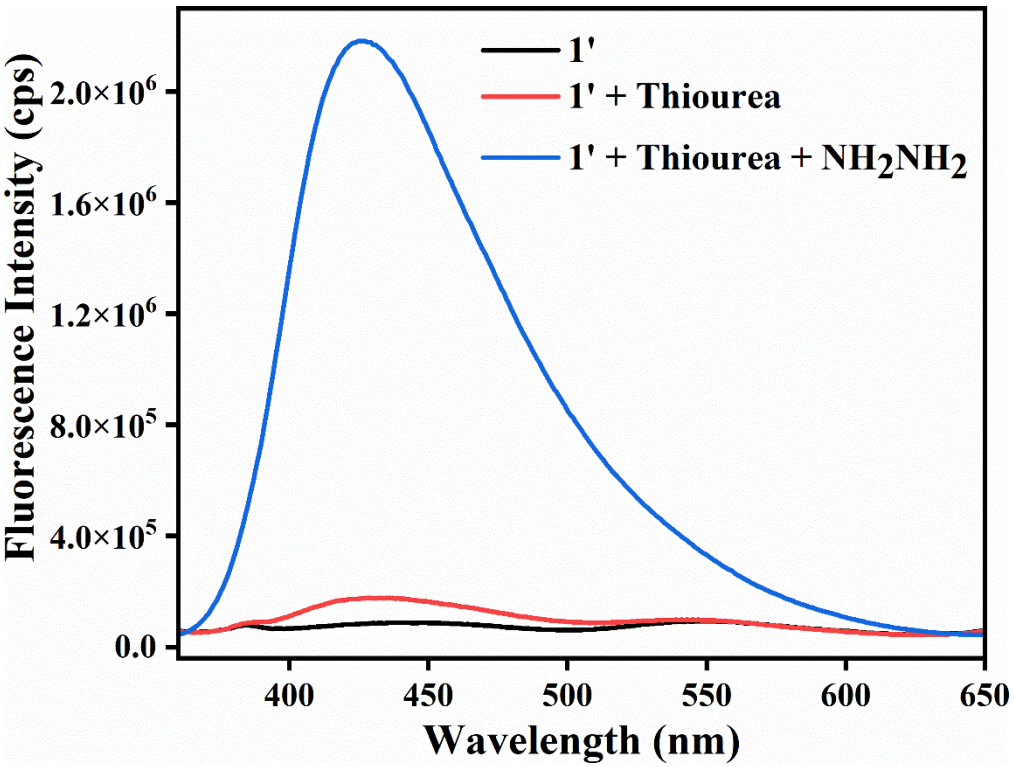

Figure S17. The fluorometric turn-on response of **1'** towards NH_2NH_2 (300 µL, 10 mM) in the presence of thiourea (300 µL, 10 mM).

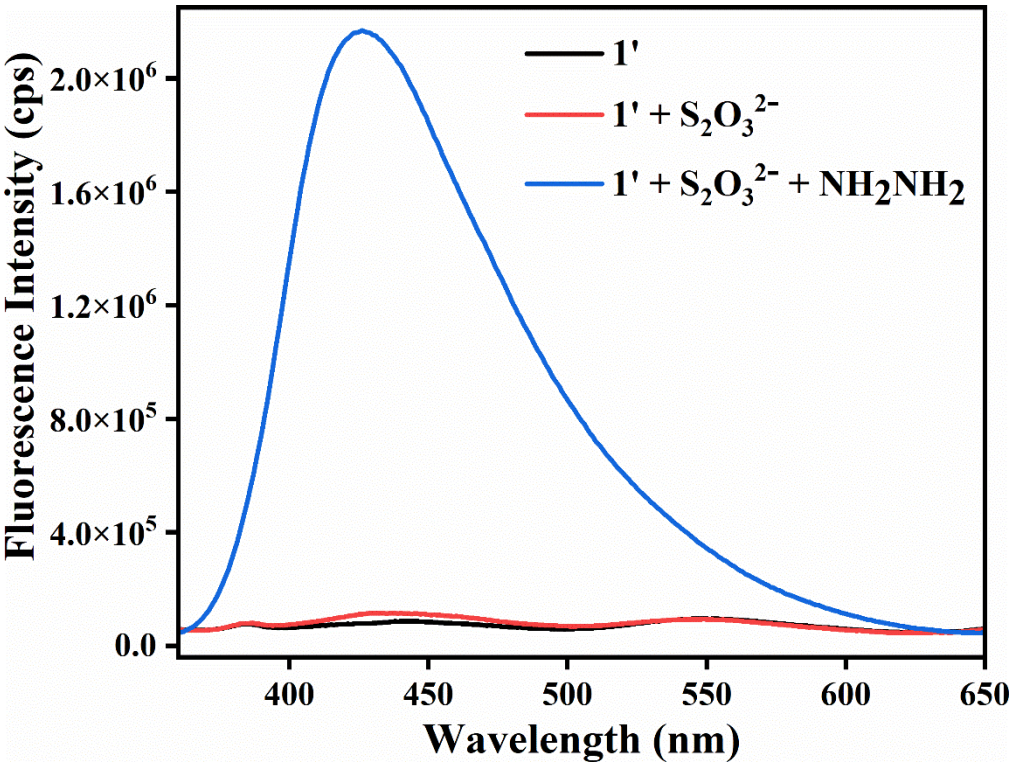

Figure S18. The fluorometric turn-on response of **1'** towards NH_2NH_2 (300 µL, 10 mM) in the presence of $S_2O_3^{2-}$ (300 µL, 10 mM).

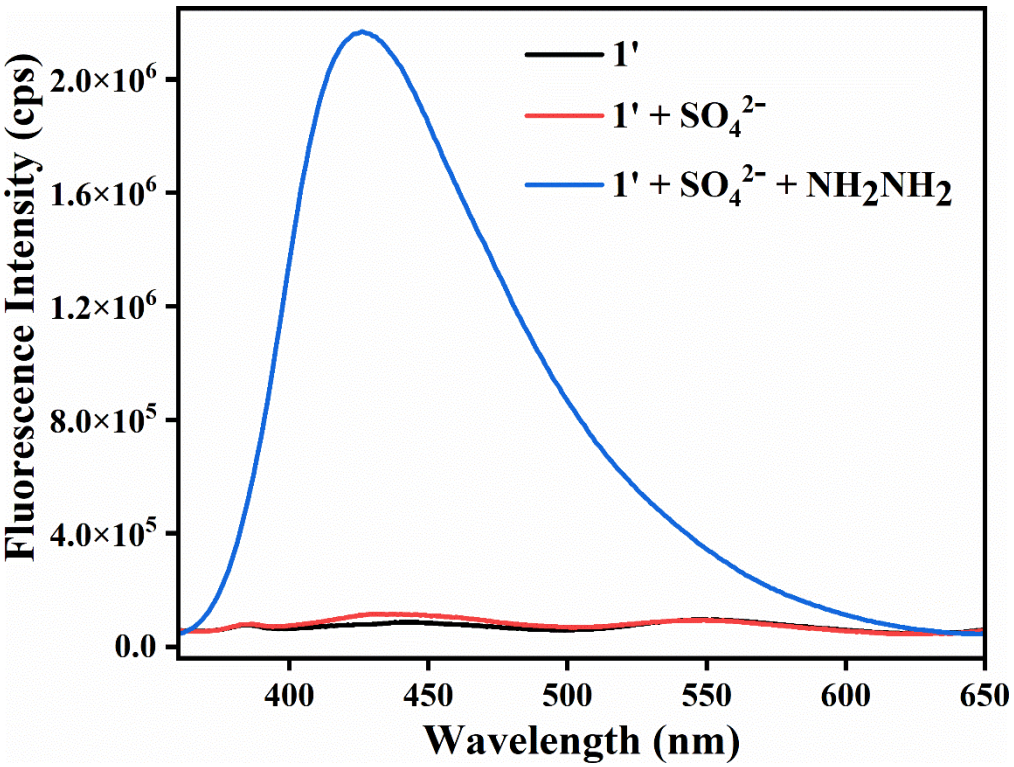

Figure S19. The fluorometric turn-on response of **1'** towards NH_2NH_2 (300 µL, 10 mM) in the presence of SO_4^{2-} (300 µL, 10 mM).

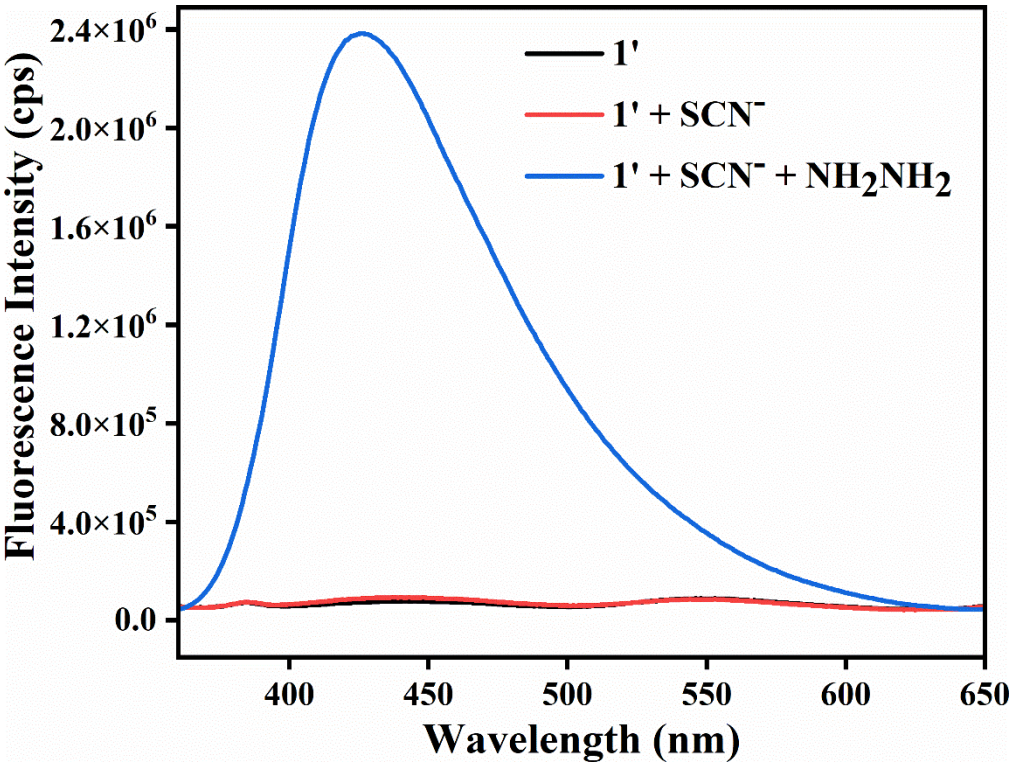

Figure S20. The fluorometric turn-on response of **1'** towards NH_2NH_2 (300 µL, 10 mM) in the presence of SCN^- (300 µL, 10 mM).

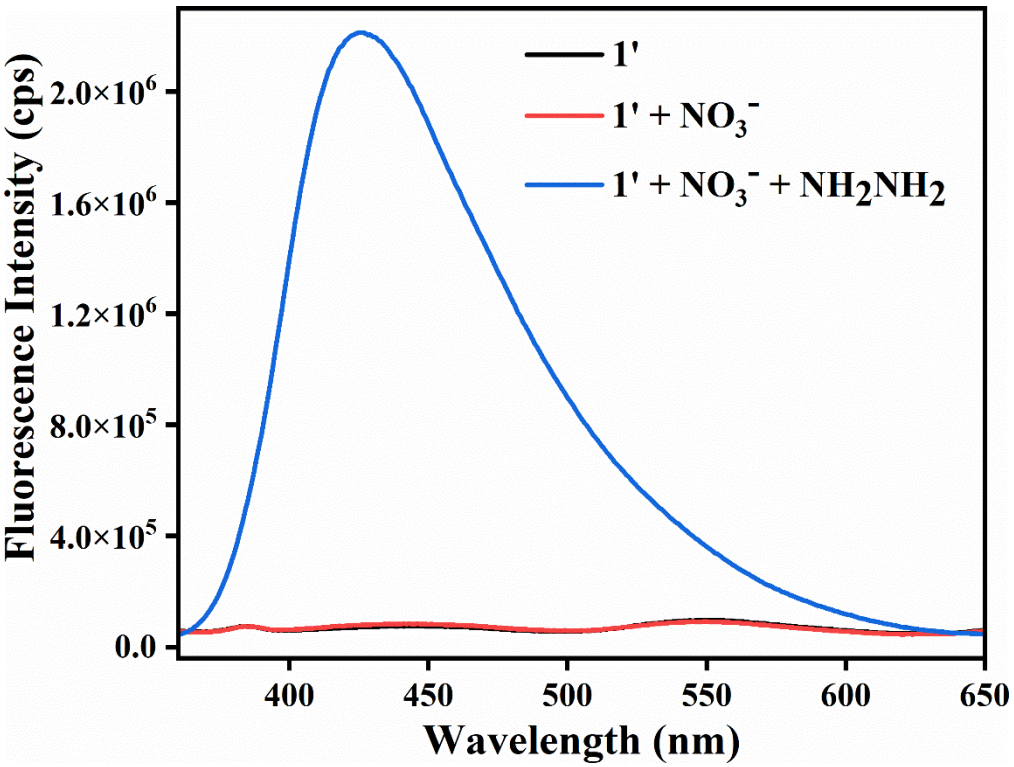

Figure S21. The fluorometric turn-on response of **1'** towards NH_2NH_2 (300 µL, 10 mM) in the presence of NO_3^- (300 µL, 10 mM).

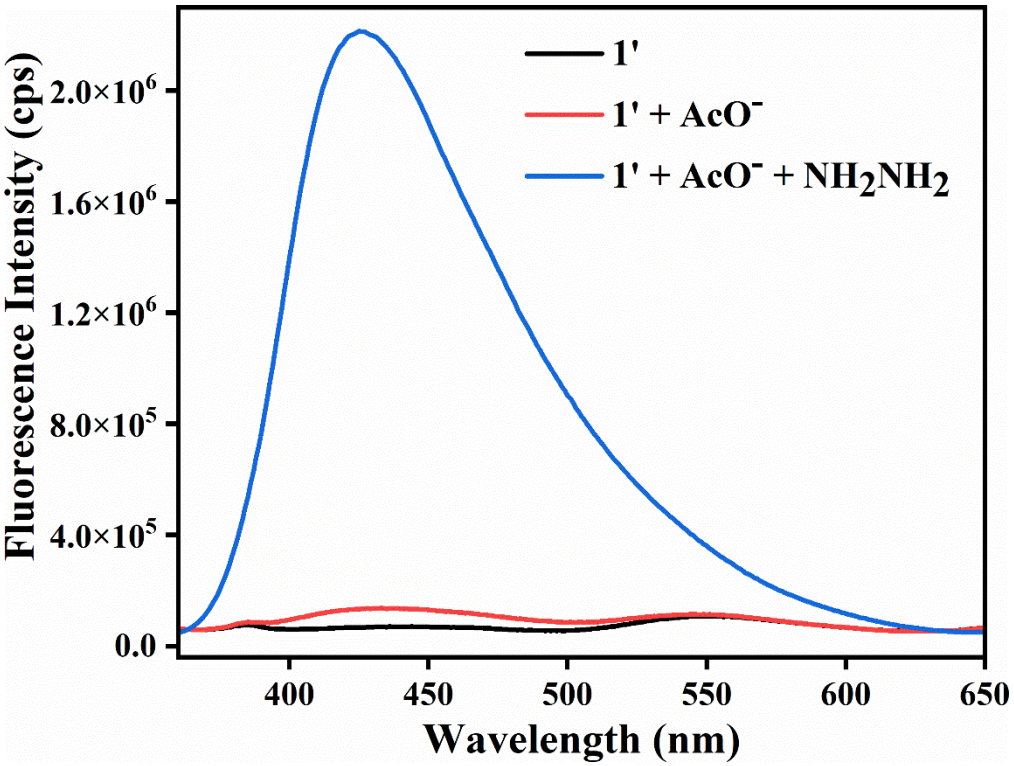

Figure S22. The fluorometric turn-on response of **1'** towards NH_2NH_2 (300 µL, 10 mM) in the presence of CH_3COO^-a (300 µL, 10 mM).

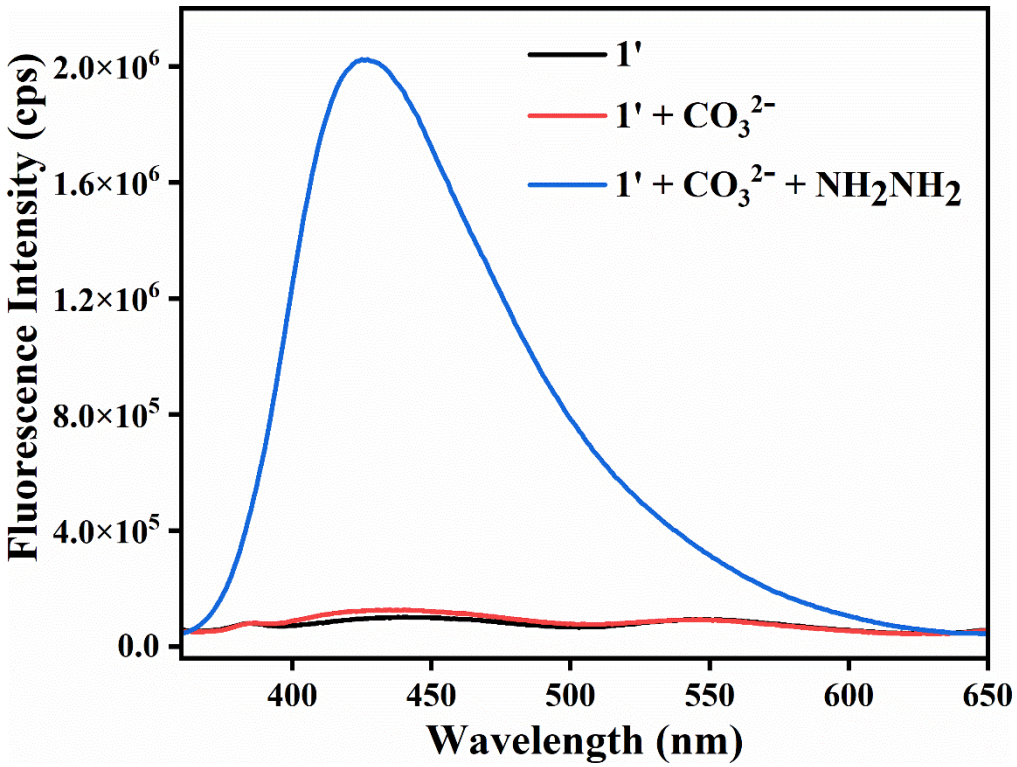

Figure S23. The fluorometric turn-on response of **1'** towards NH_2NH_2 (300 µL, 10 mM) in the presence of CO_3^{2-} (300 µL, 10 mM).

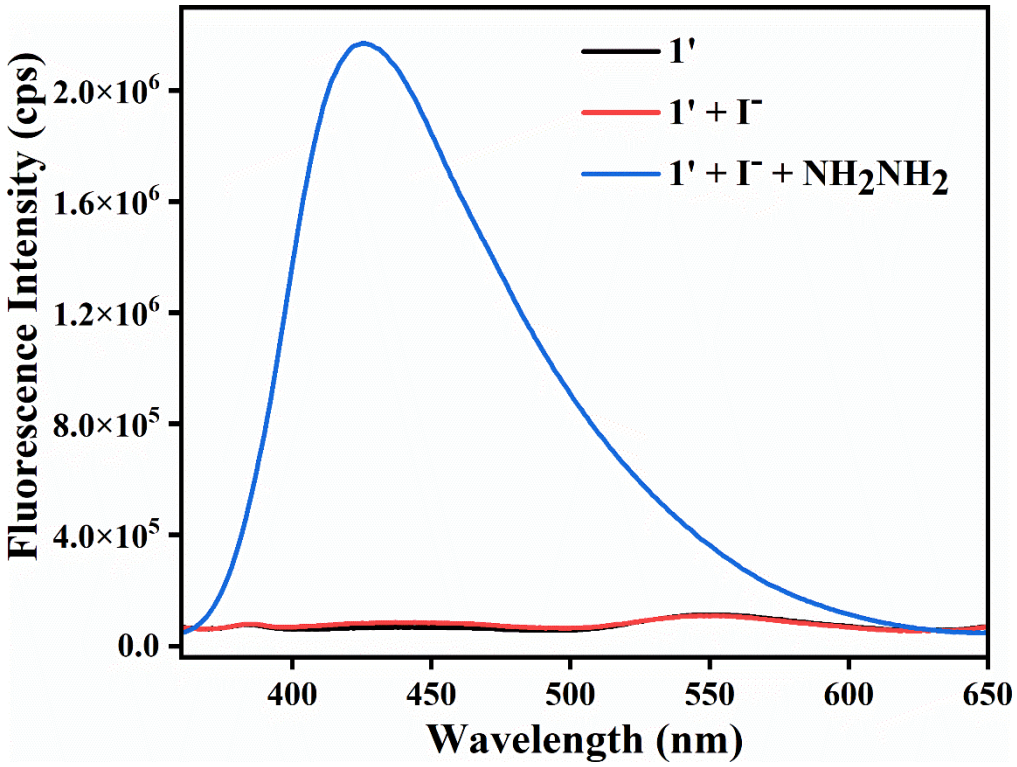

Figure S24. The fluorometric turn-on response of **1'** towards NH_2NH_2 (300 µL, 10 mM) in the presence of I^- (300 µL, 10 mM).

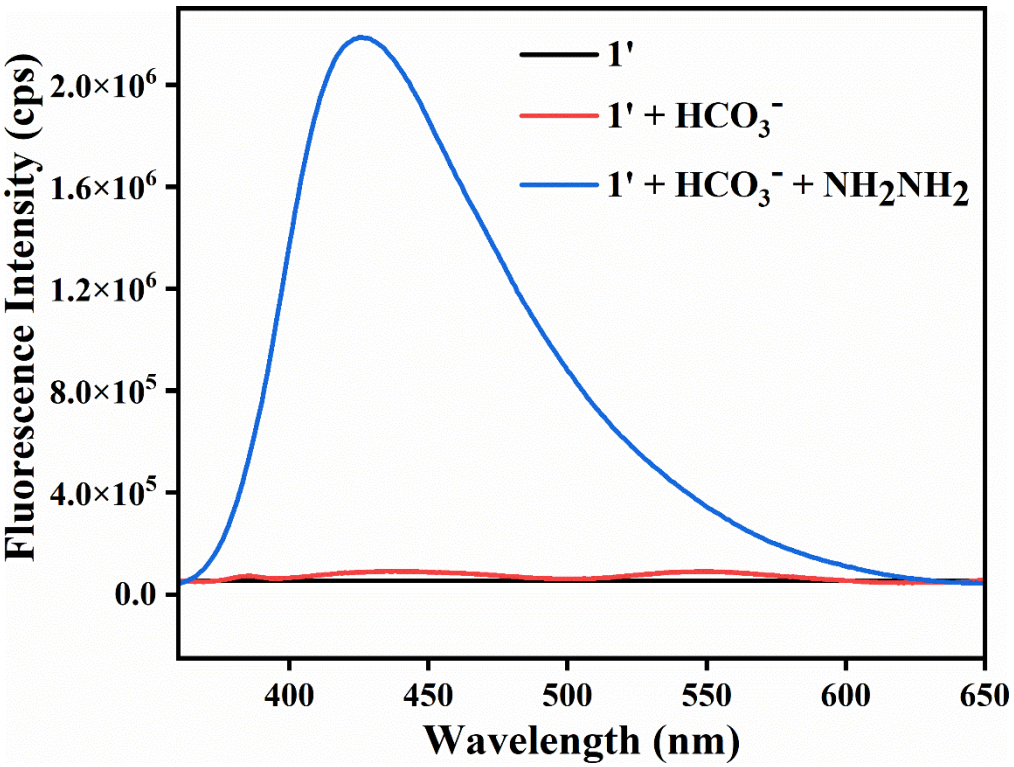

Figure S25. The fluorometric turn-on response of **1'** towards NH_2NH_2 (300 µL, 10 mM) in the presence of HCO_3^- (300 µL, 10 mM).

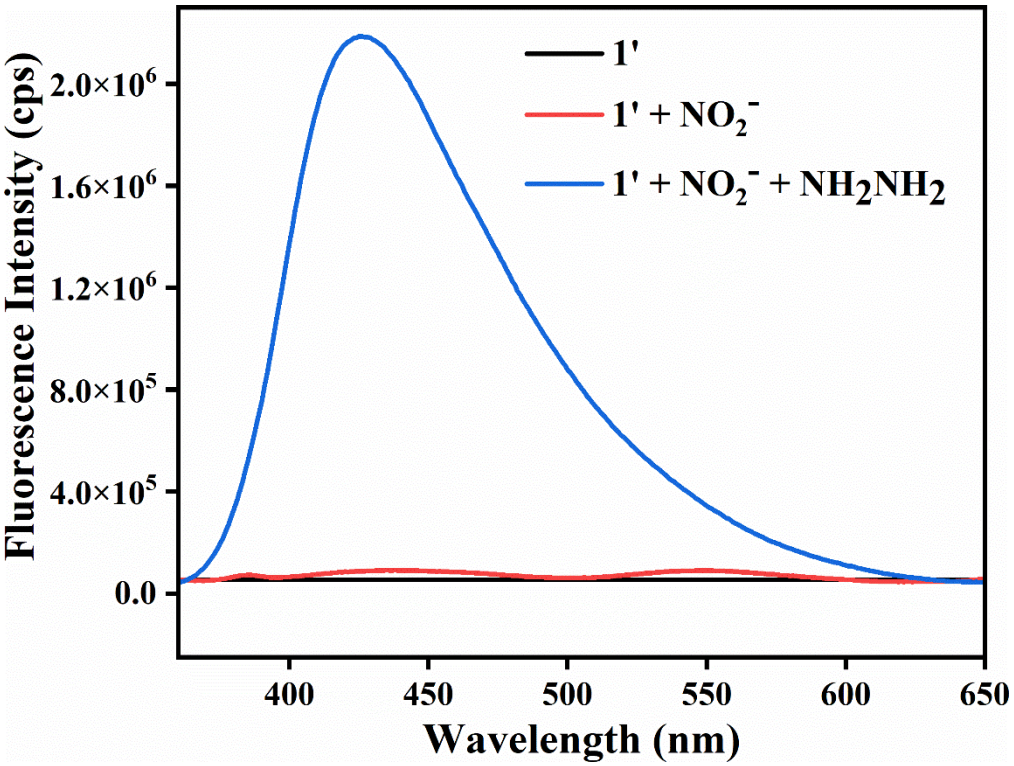

Figure S26. The fluorometric turn-on response of **1'** towards NH_2NH_2 (300 µL, 10 mM) in the presence of NO_2^- (300 µL, 10 mM).

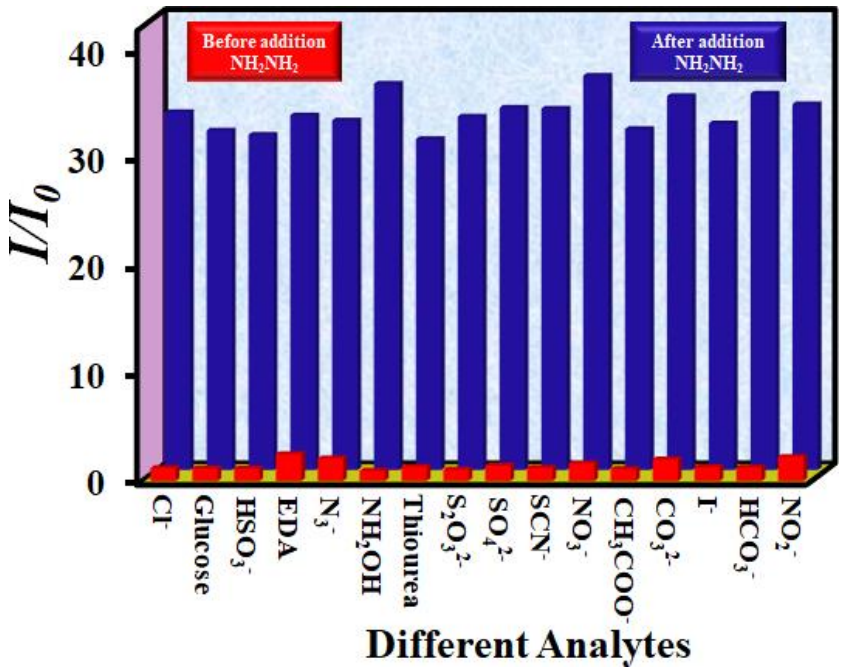

Figure S27. Selectivity of **1'** towards NH_2NH_2 in the presence of other interfering analytes.

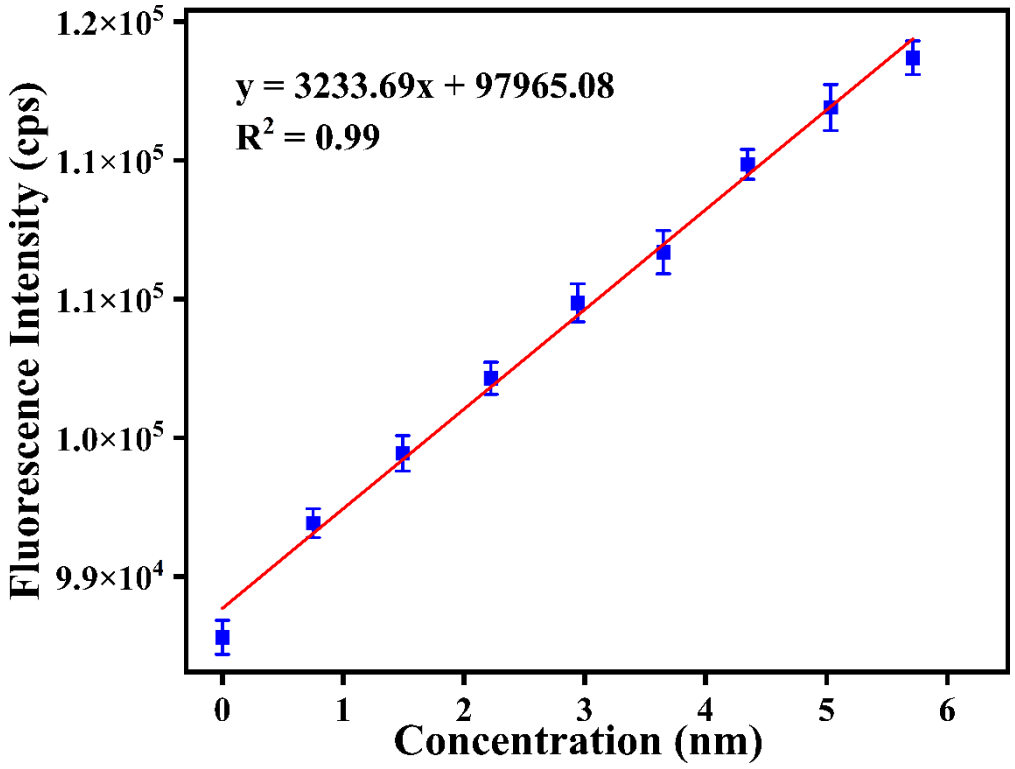

Figure S28. Change in the fluorescence intensity of **1'** in water as a function of concentration of NH_2NH_2 (with error bar).

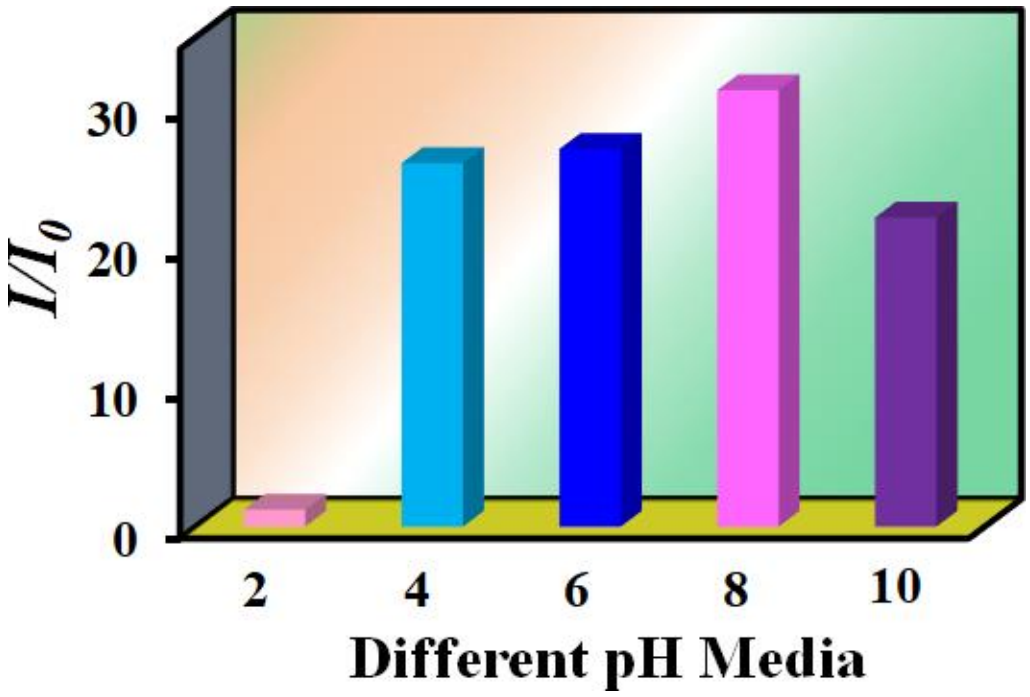

Figure S29. Detection of NH_2NH_2 in different pH media.

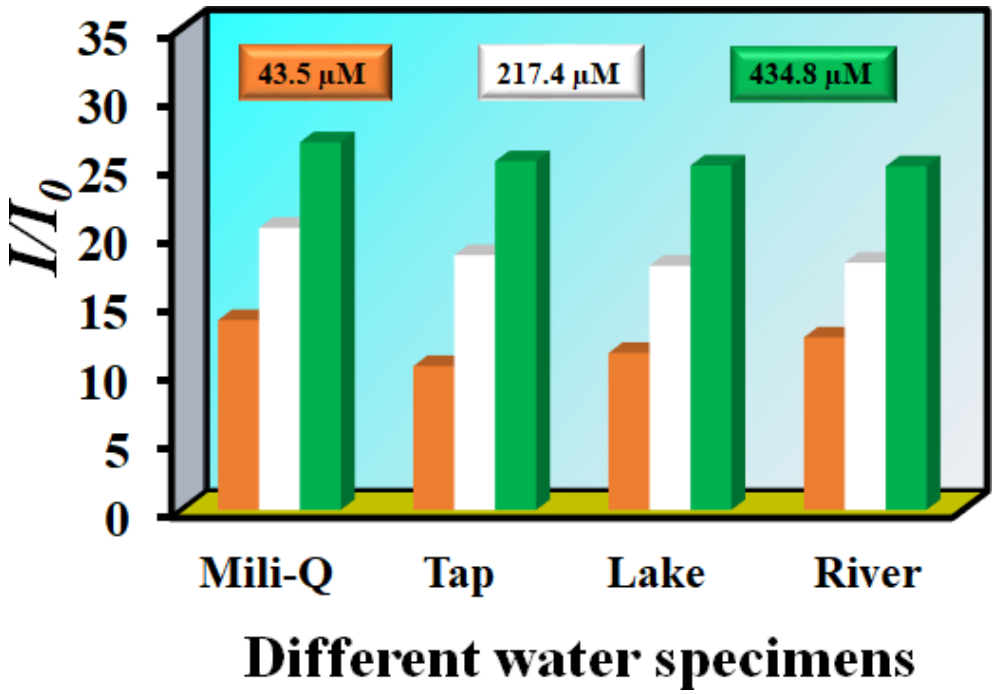

Figure S30. Detection of NH_2NH_2 in various real water specimen with different concentration.

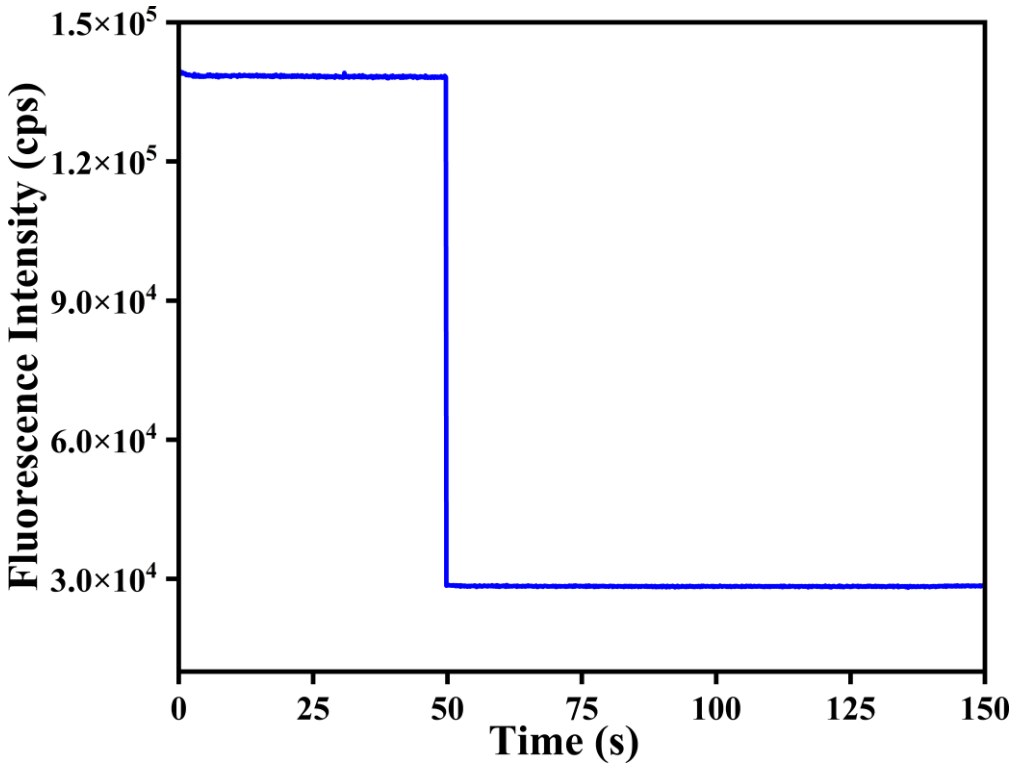

Figure S31. Fluorescence kinetic experiment for nicardipine sensing.

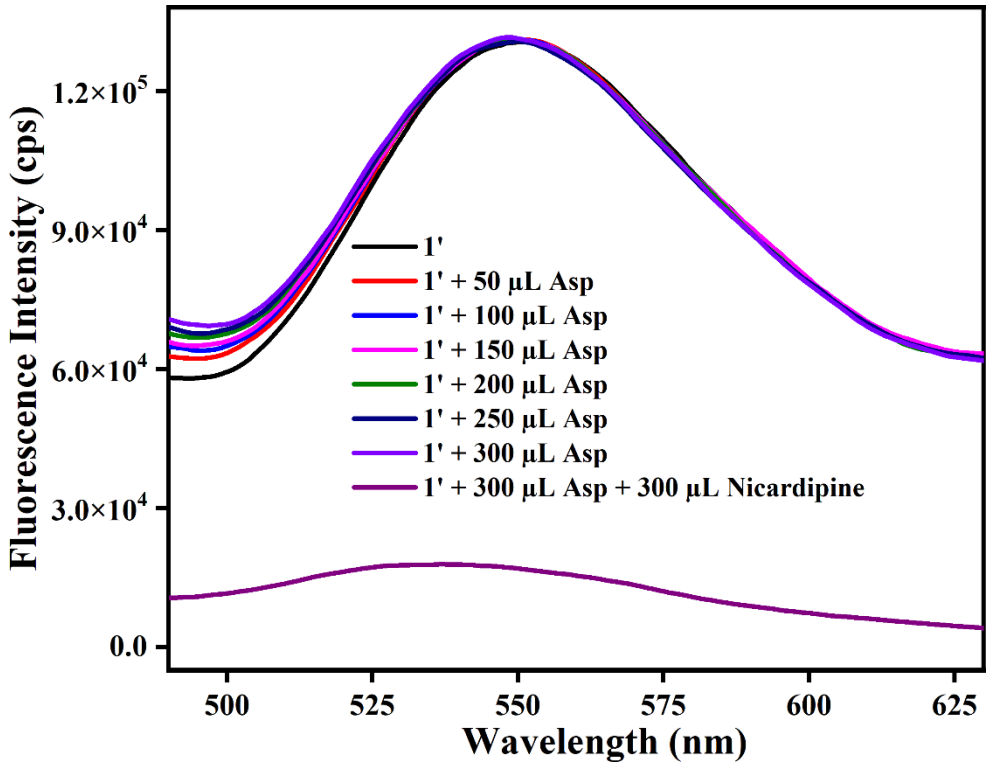

Figure S32. The fluorometric turn-off response of **1'** towards nicardipine presence of aspartic acid (300 µL, 5 mM).

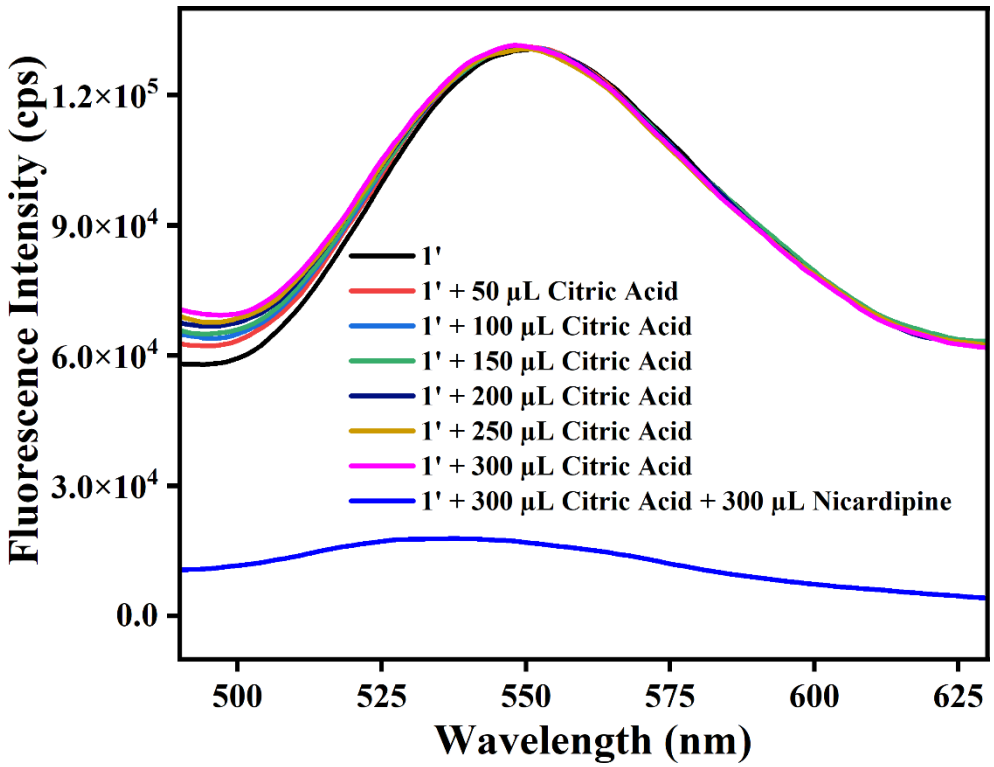

Figure S33. The fluorometric turn-off response of **1'** towards nicardipine presence of citric acid.

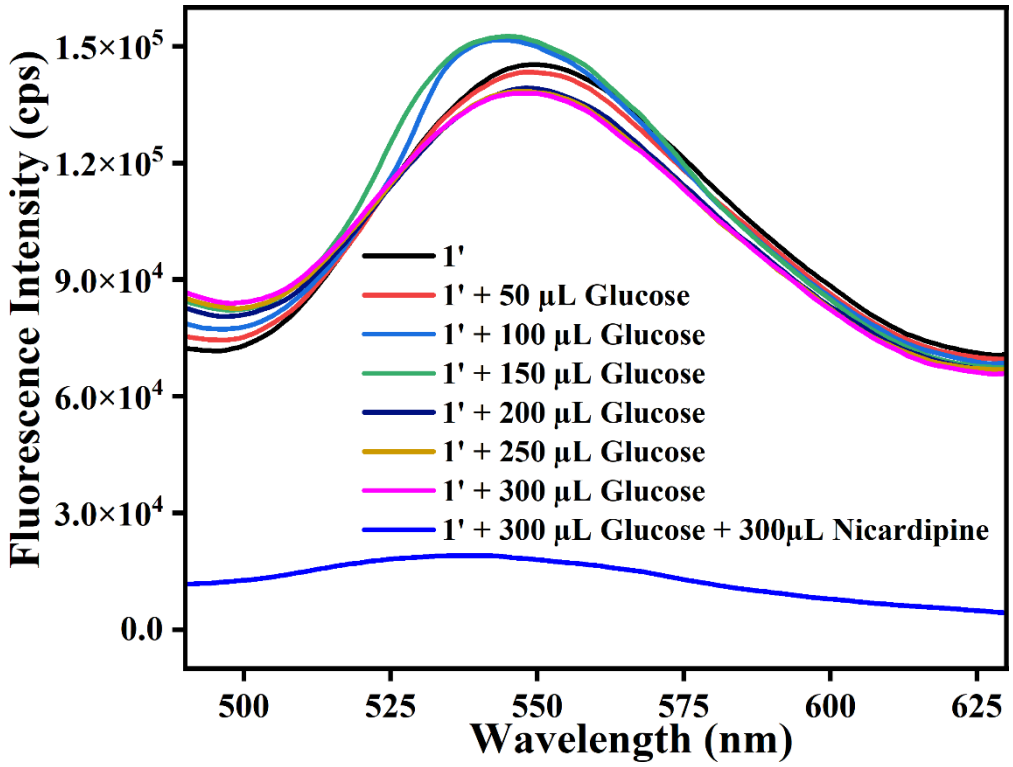

Figure S34. The fluorometric turn-off response of **1'** towards nicardipine presence of glucose.

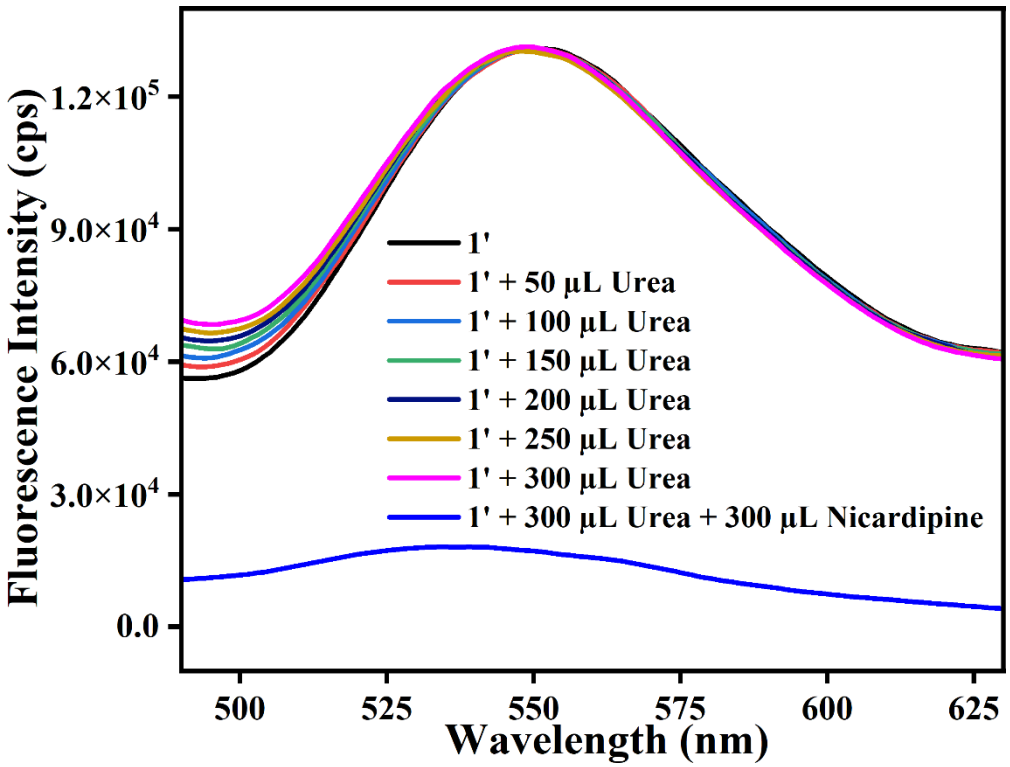

Figure S35. The fluorometric turn-off response of **1'** towards nicardipine presence of urea.

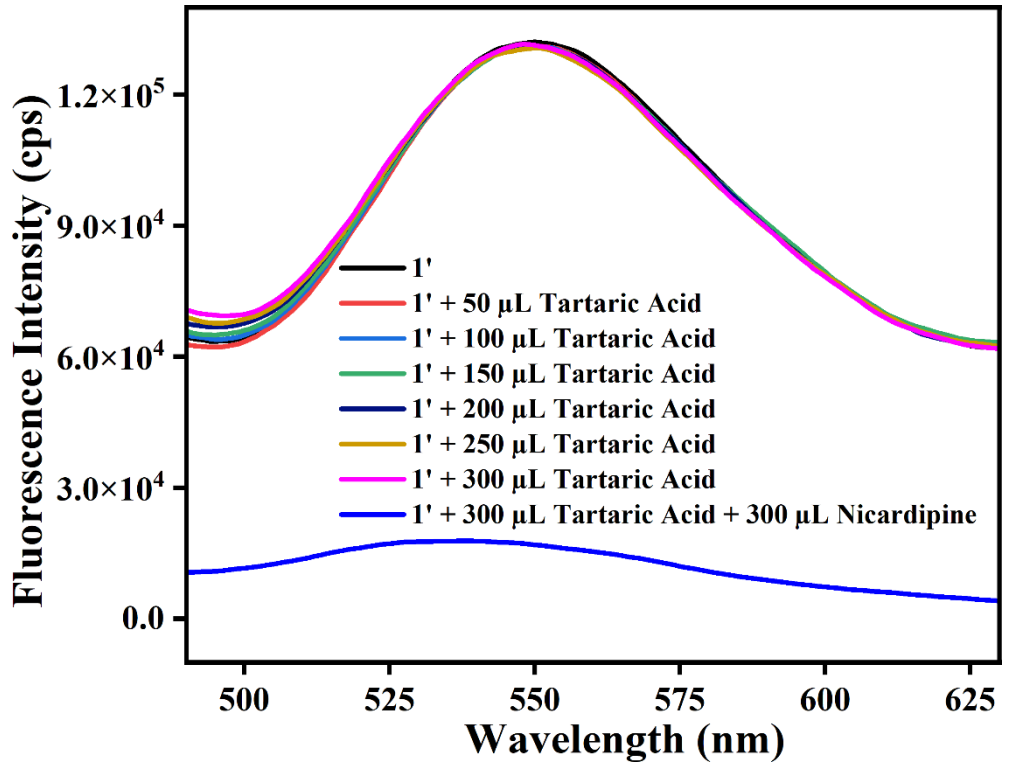

Figure S36. The fluorometric turn-off response of **1'** towards nicardipine presence of tartaric acid.

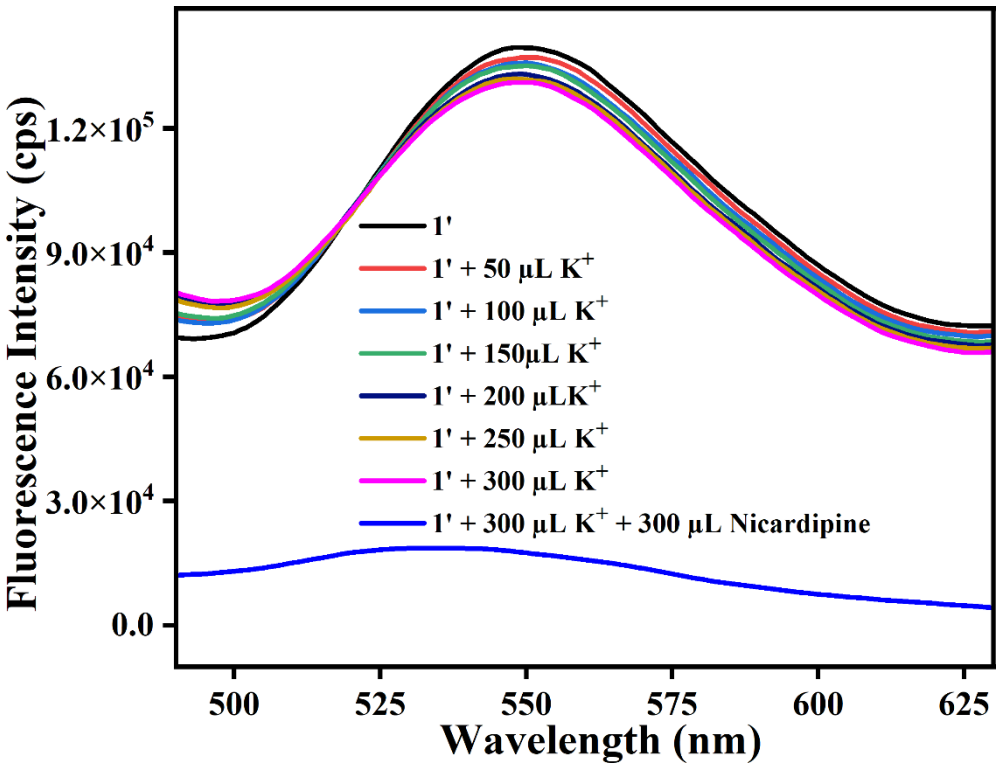

Figure S37. The fluorometric turn-off response of **1'** towards nicardipine the presence of K^+.

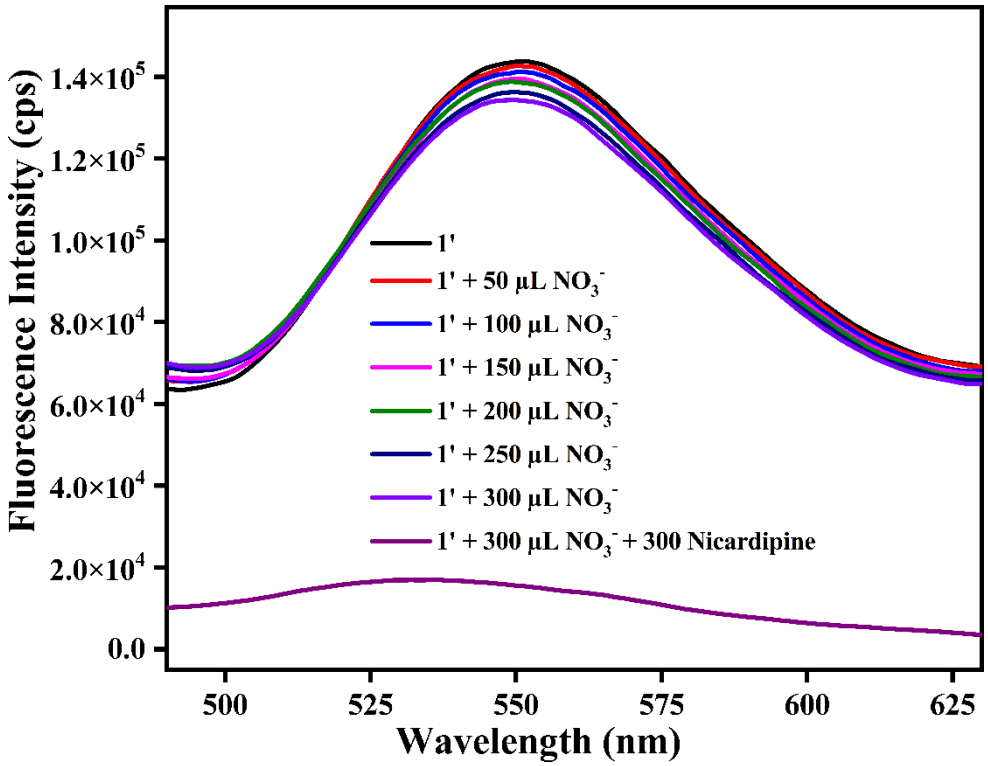

Figure S38. The fluorometric turn-off response of **1'** towards nicardipine(300 µL, 5 mM) in the presence of NO_3^- (300 µL, 5 mM).

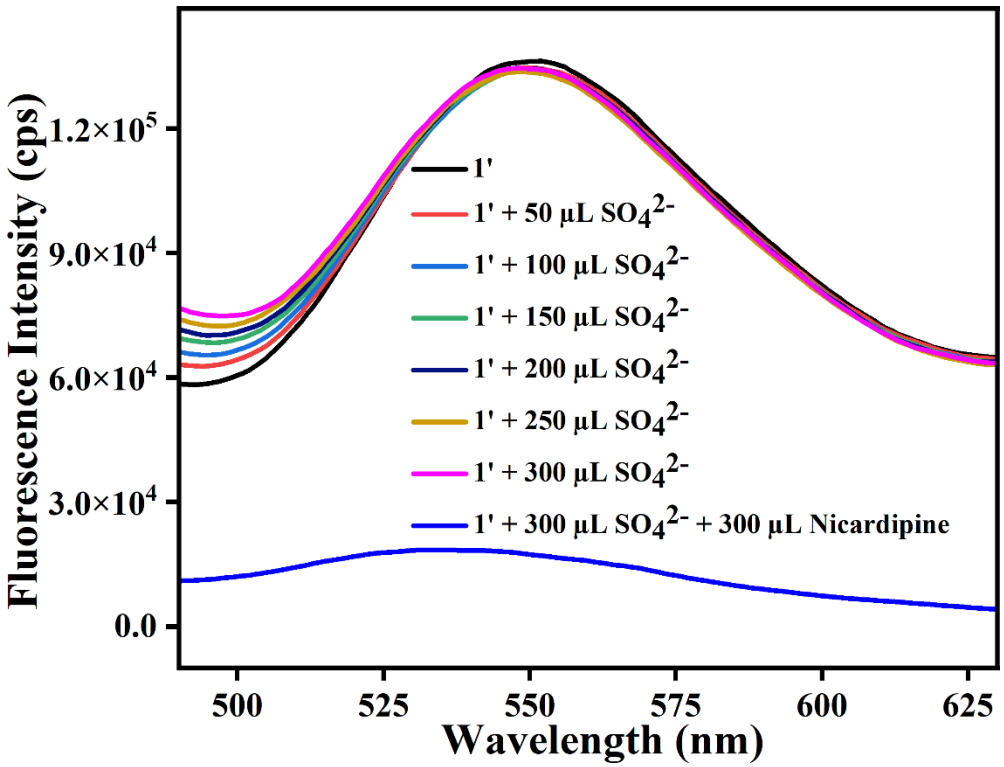

Figure S39. The fluorometric turn-off response of **1'** towards nicardipine presence of SO_4^{2-}.

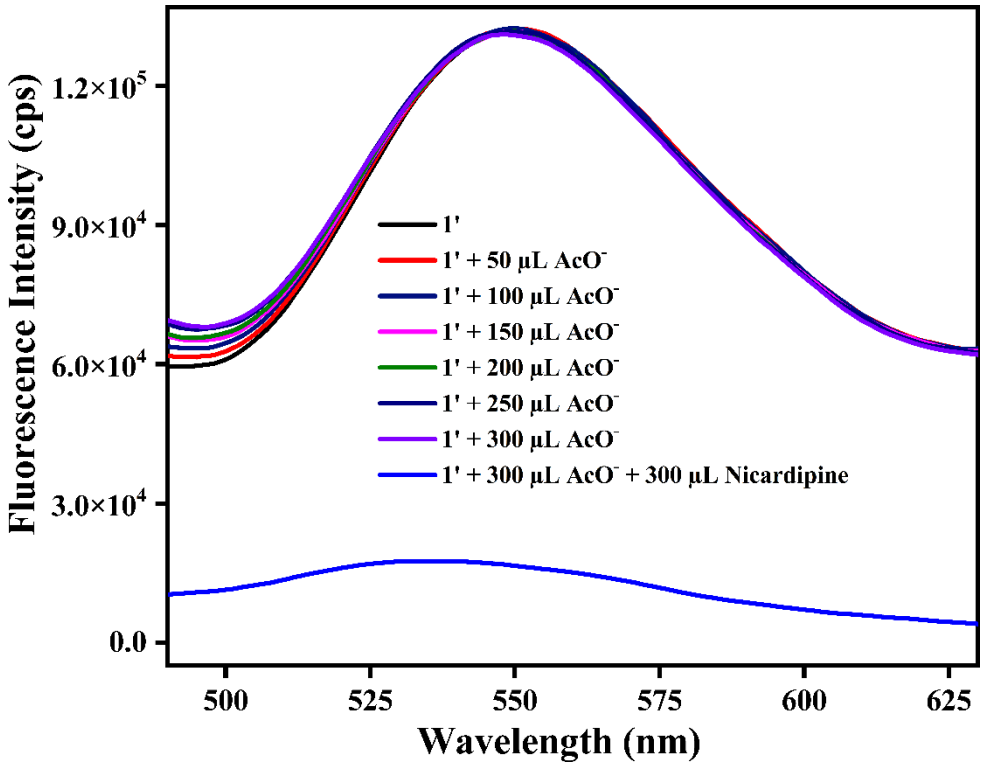

Figure S40. The fluorometric turn-off response of **1'** towards nicardipine presence of CH_3COO^-.

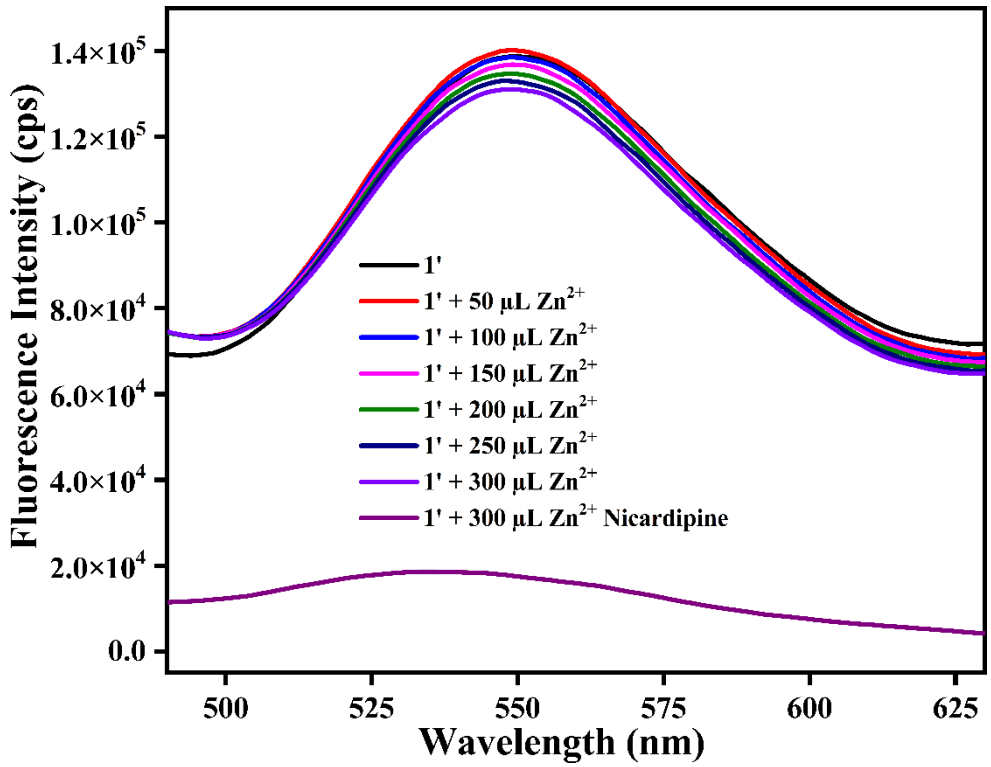

Figure S41. The fluorometric turn-off response of **1'** towards nicardipine(300 µL, 5 mM) in the presence of Zn^{2+} (300 µL, 5 mM).

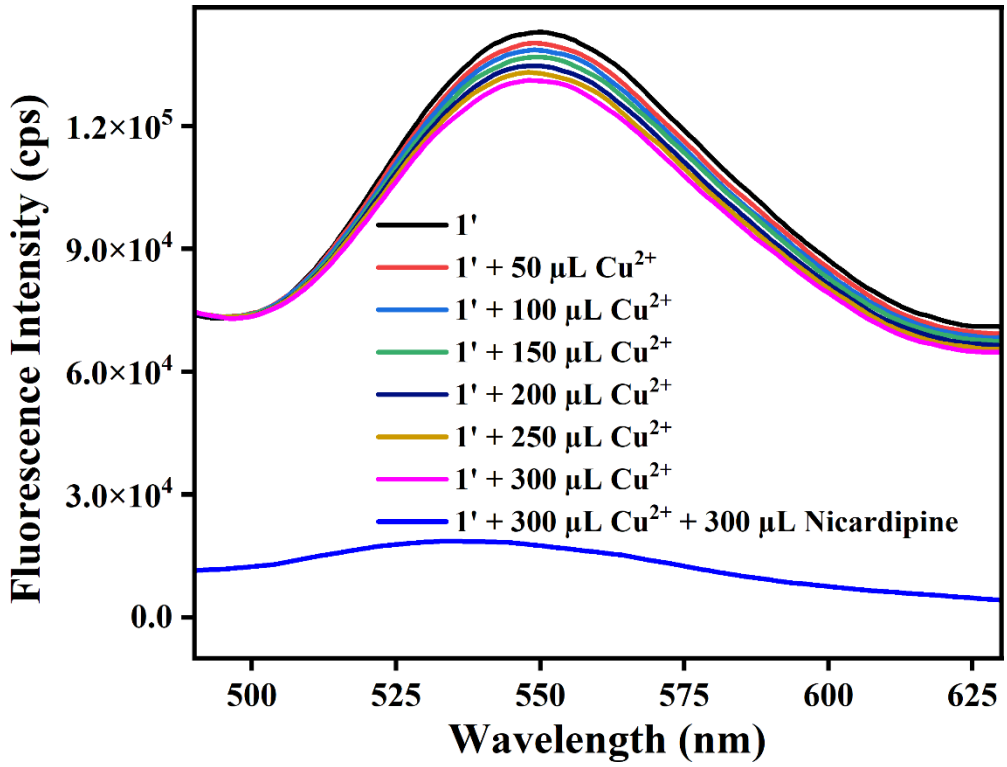

Figure S42. The fluorometric turn-off response of **1'** towards nicardipine presence of Cu^{2+}.

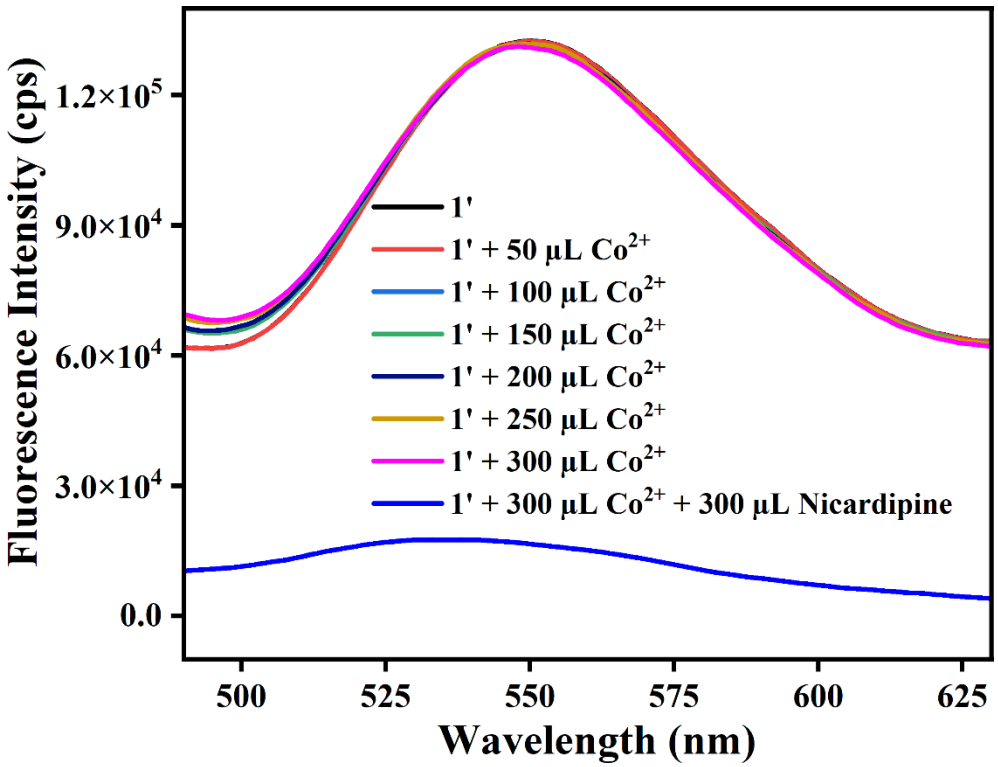

Figure S43. The fluorometric turn-off response of **1'** towards nicardipine presence of Co^{2+}.

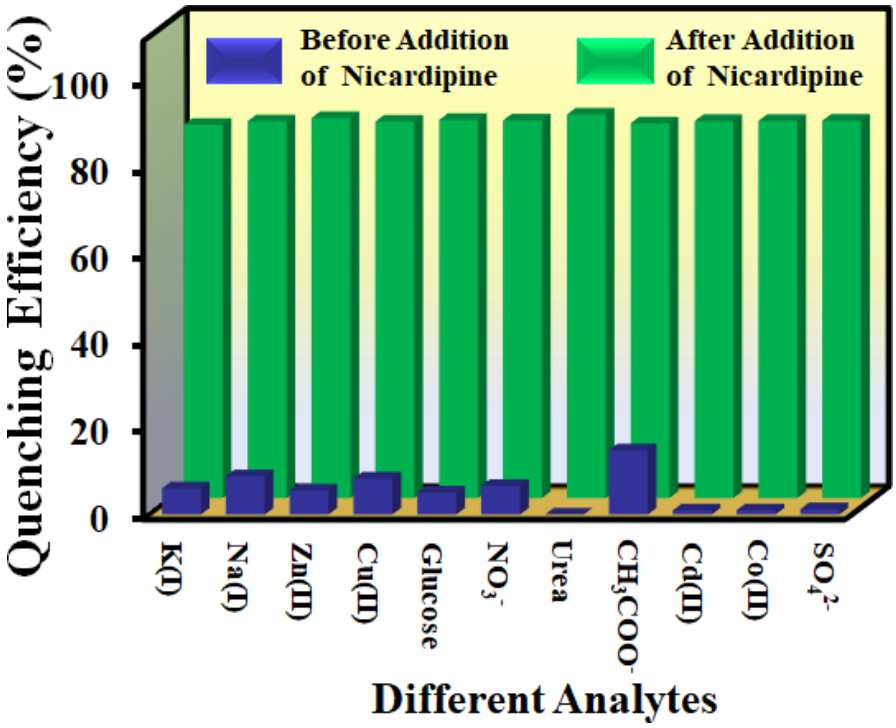

Figure S44. Selectivity of **1'** towards nicardipine sensing in the presence of other analytes.

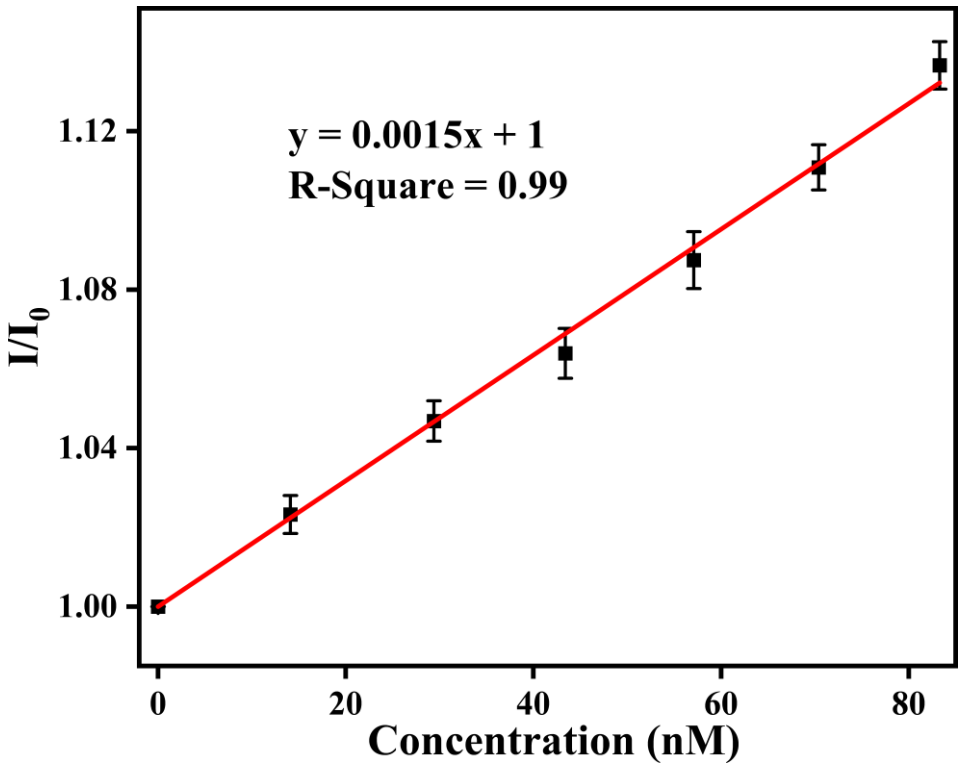

Figure S45. Stern-Volmer plot for the fluorrometric sensing of nicardipine using the probe **1'** (with error bars).

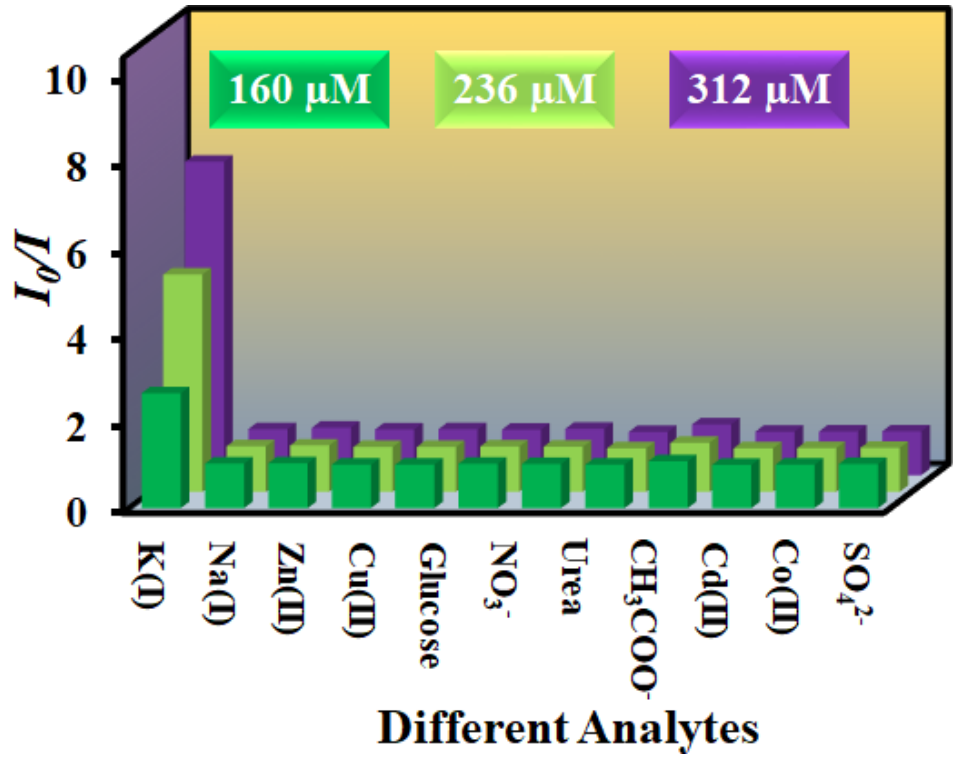

Figure S46. 3-D Stern-Volmer plots for nicardipine sensing.

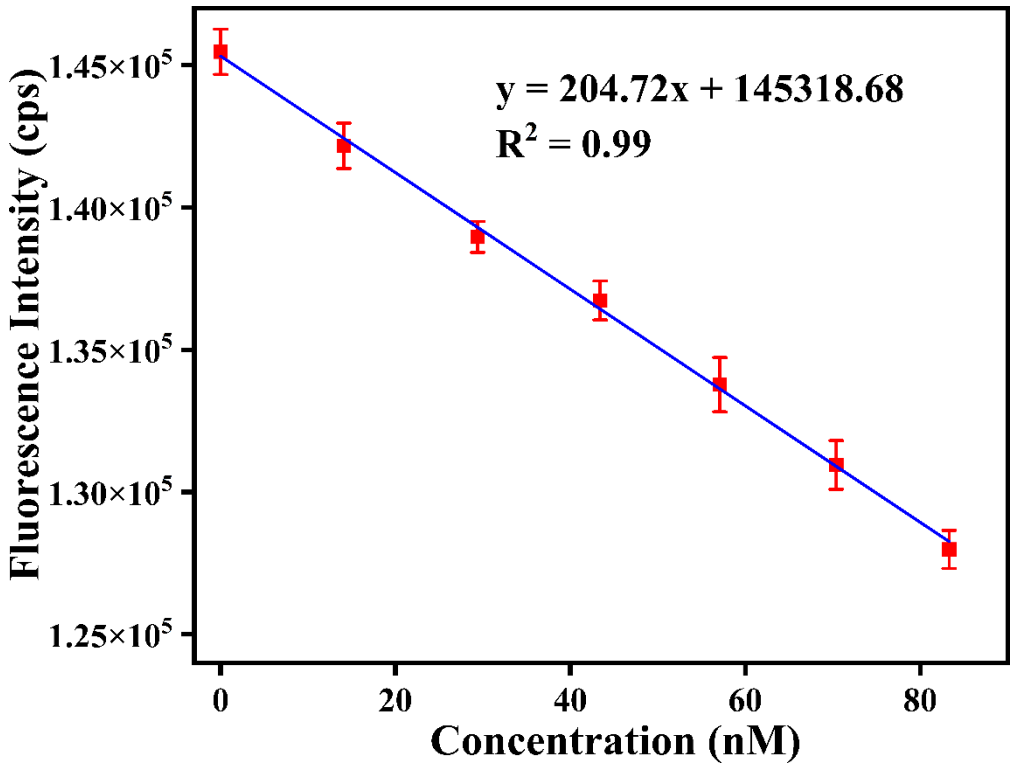

Figure S47. Change in the fluorescence intensity of **1'** in water as a function of concentration of nicardipine (with error bar).

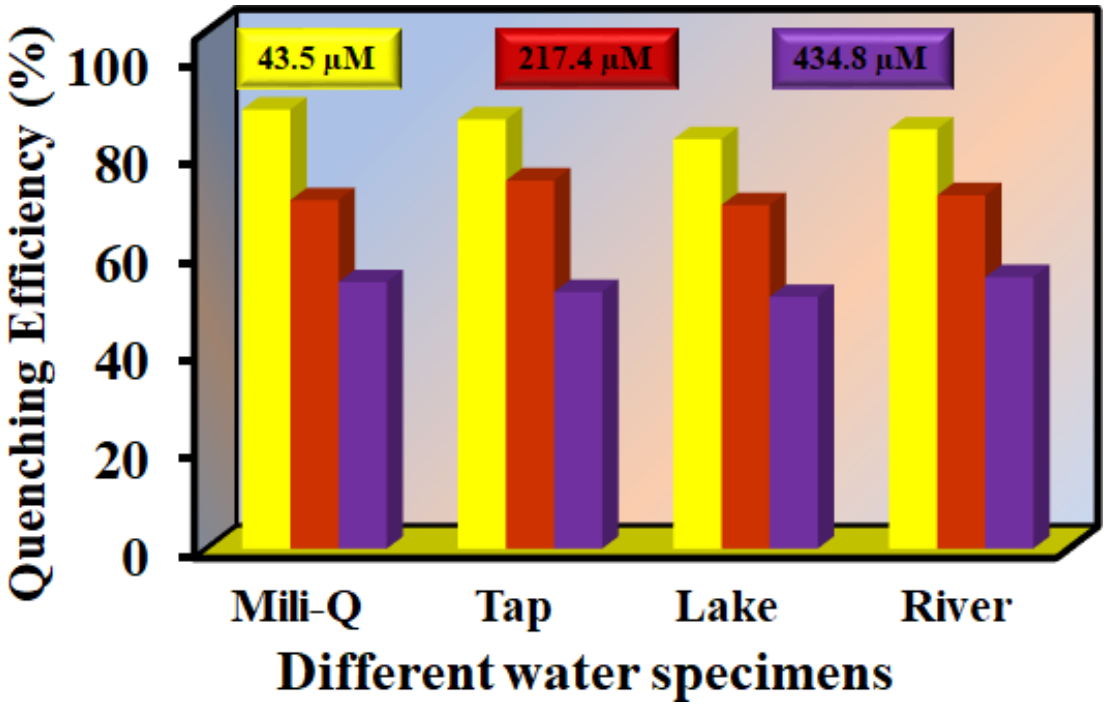

Figure S48. Detection of nicardipine in various wastewater specimens at different concentrations.

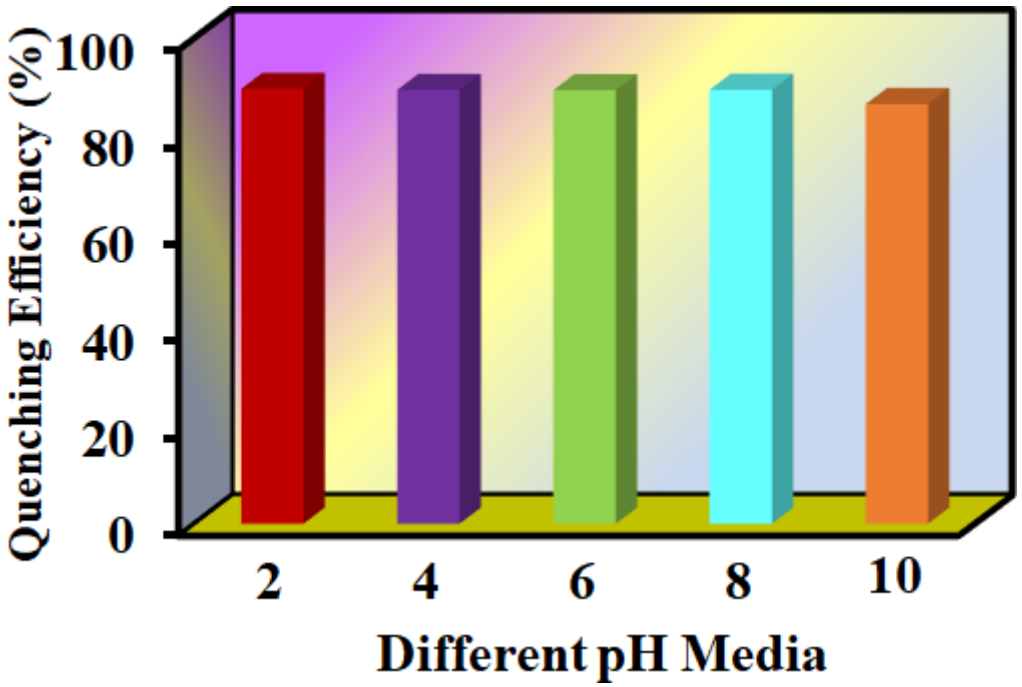

Figure S49. Nicardipine detection in different pH media.

Table S1. Fluorometric detection of nicardipine human serum sample by **1'**.

Nicardipine Spiked (µM)	Nicardipine Found (µM)	Recovery (%)	RSD (%) (n=3)
9.58	10.08	105.21	1.08
18.99	18.27	96.20	0.95
28.21	28.39	100.64	1.51

Table S2. Fluorometric detection of nicardipine human urine sample by **1'**.

Nicardipine Spiked (µM)	Nicardipine Found (µM)	Recovery (%)	RSD (%) (n=3)
9.58	10.13	105.74	1.55
18.99	19.29	101.58	0.86
28.21	27.81	98.58	1.87

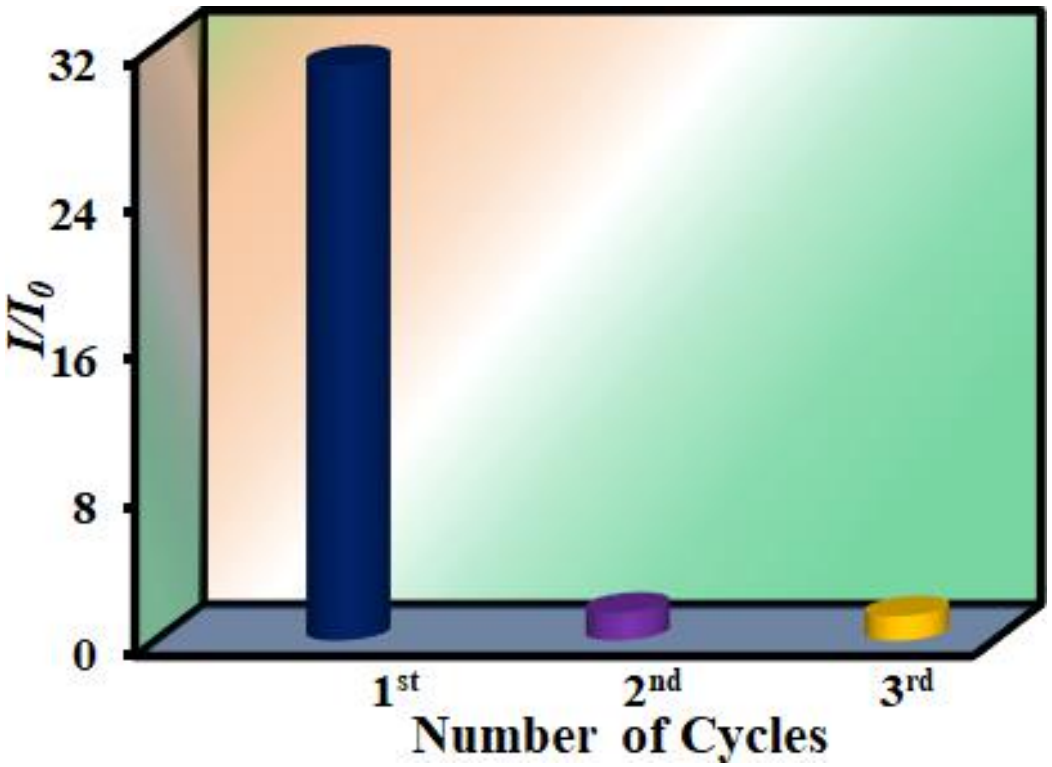

Figure S50. Reusability of the probe **1'** towards NH_2NH_2 sensing in aqueous medium.

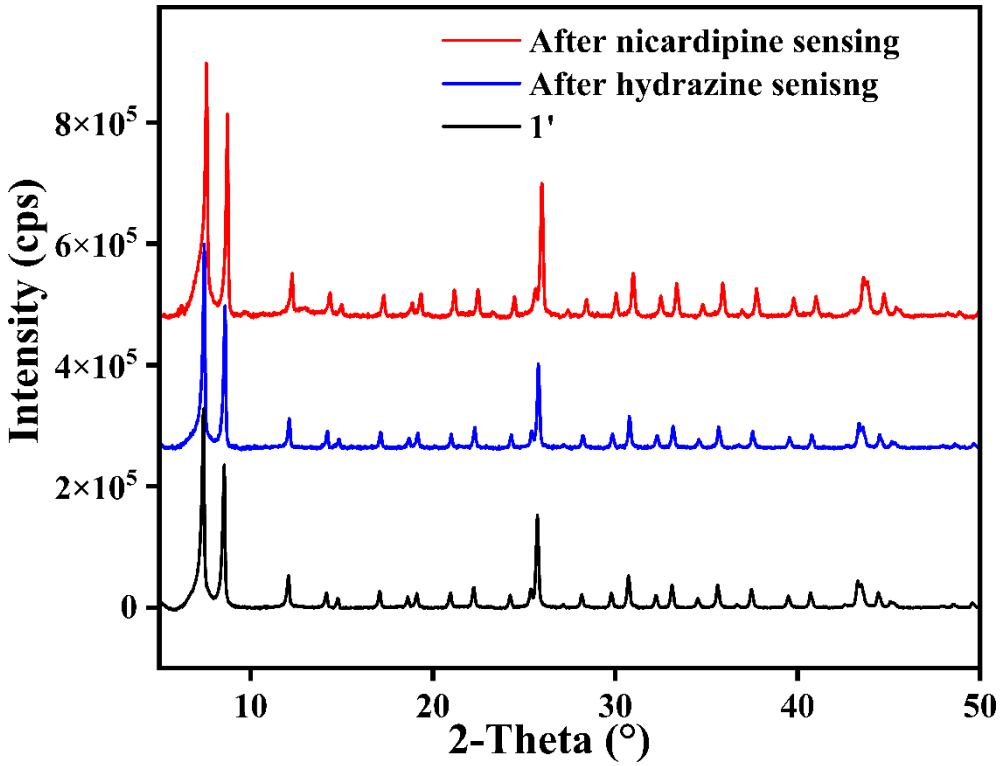

Figure S51. PXRD patterns of **1'** before and after sensing of NH_2NH_2 and nicardipine.

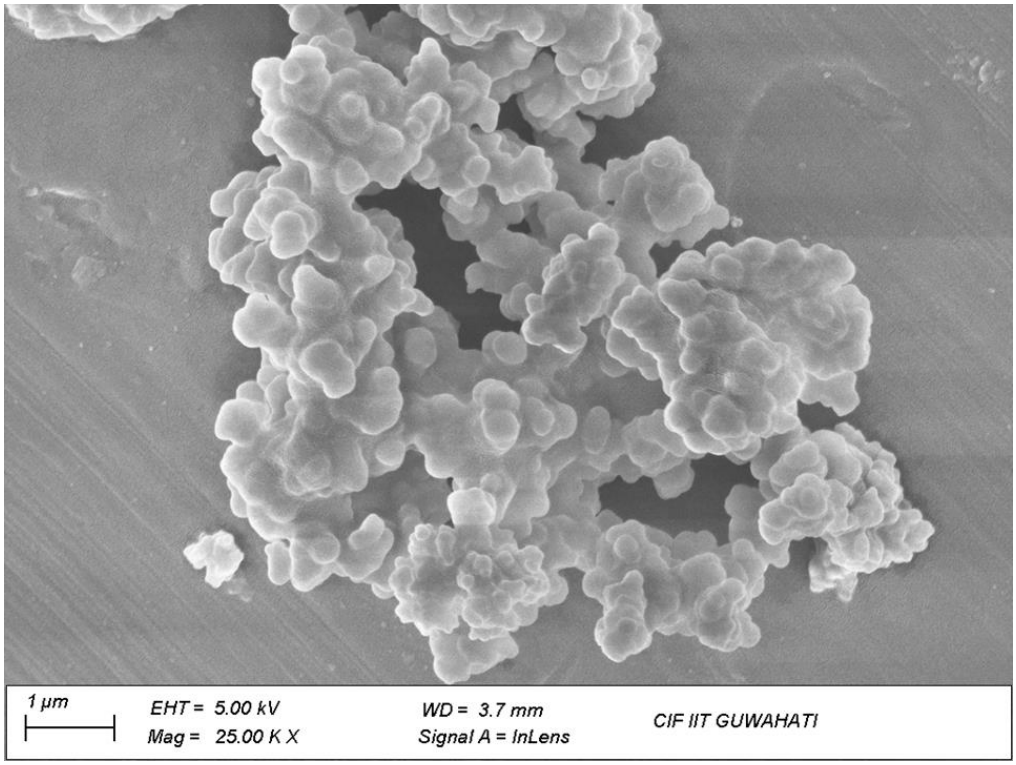

Figure S52. FESEM image of **1'** after hydrazine sensing.

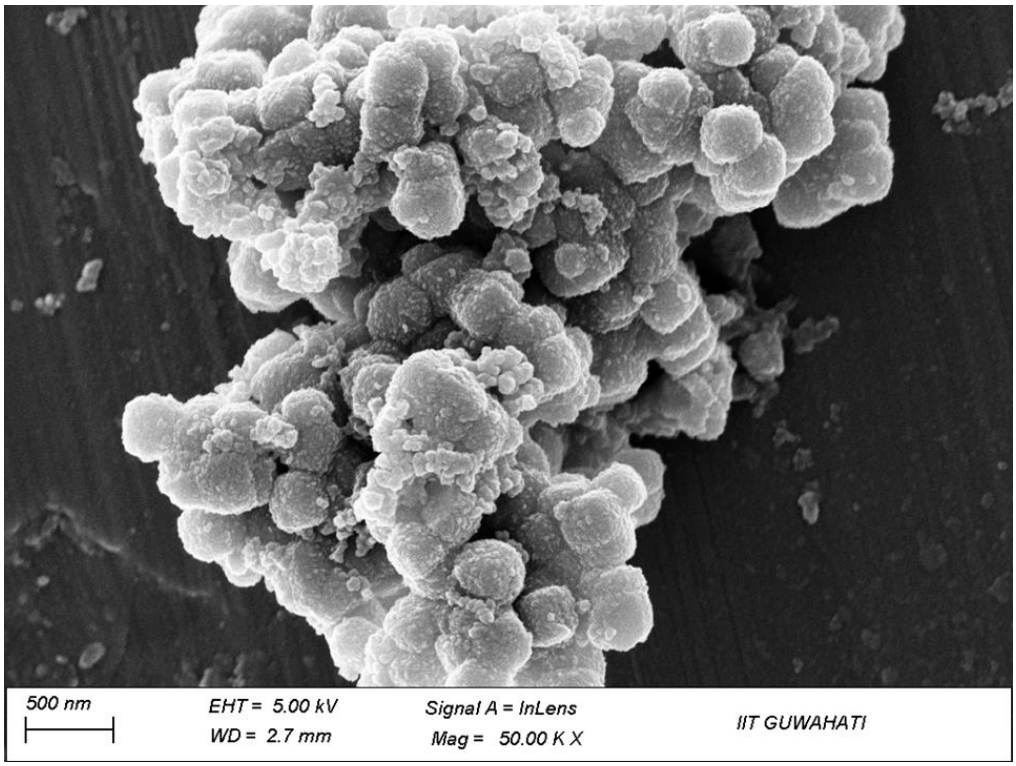

Figure S53. FESEM image of **1'** after nicardipine sensing.

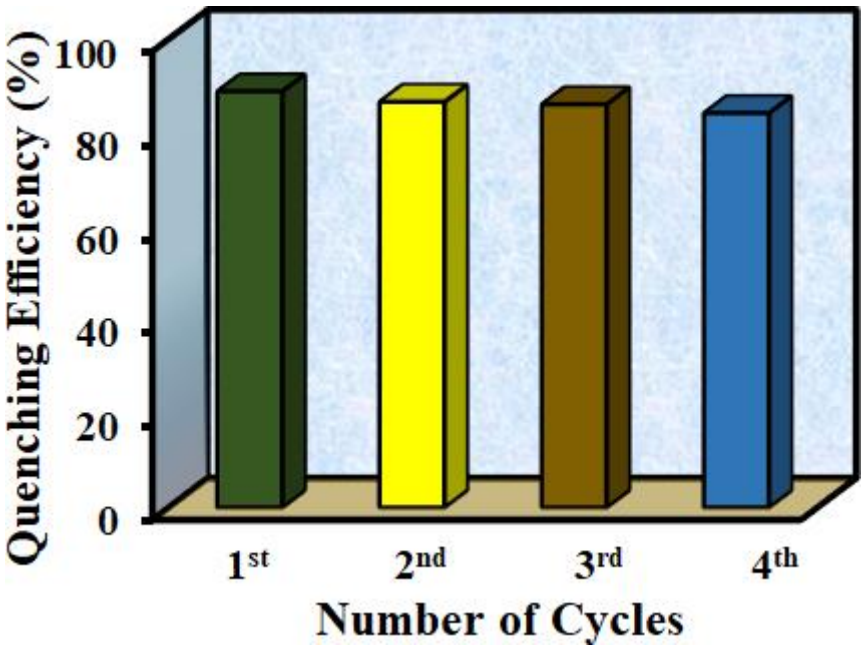

Figure S54. Reusability of the probe **1'** towards nicardipine sensing in aqueous medium.

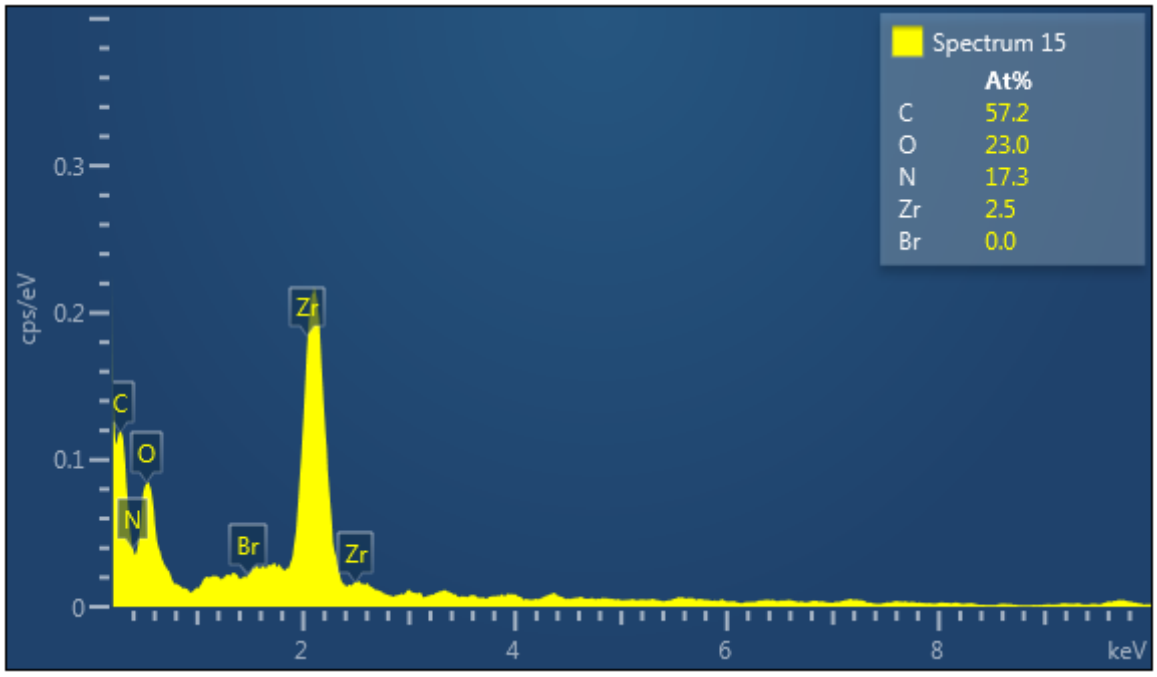

Fig. S55. EDX spectrum of **1'** after the treatmet of NH_2NH_2.

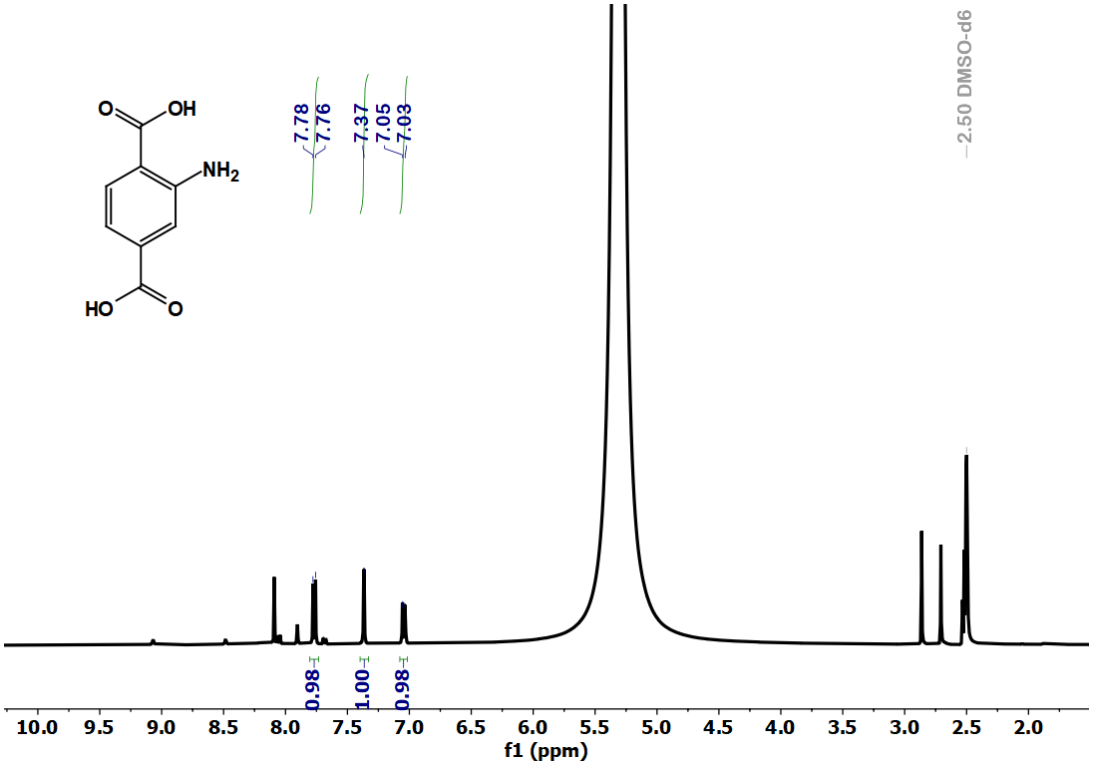

Figure S56. ^{1}H NMR spectrum of digested obtained **1'** after treatment of NH_2NH_2.

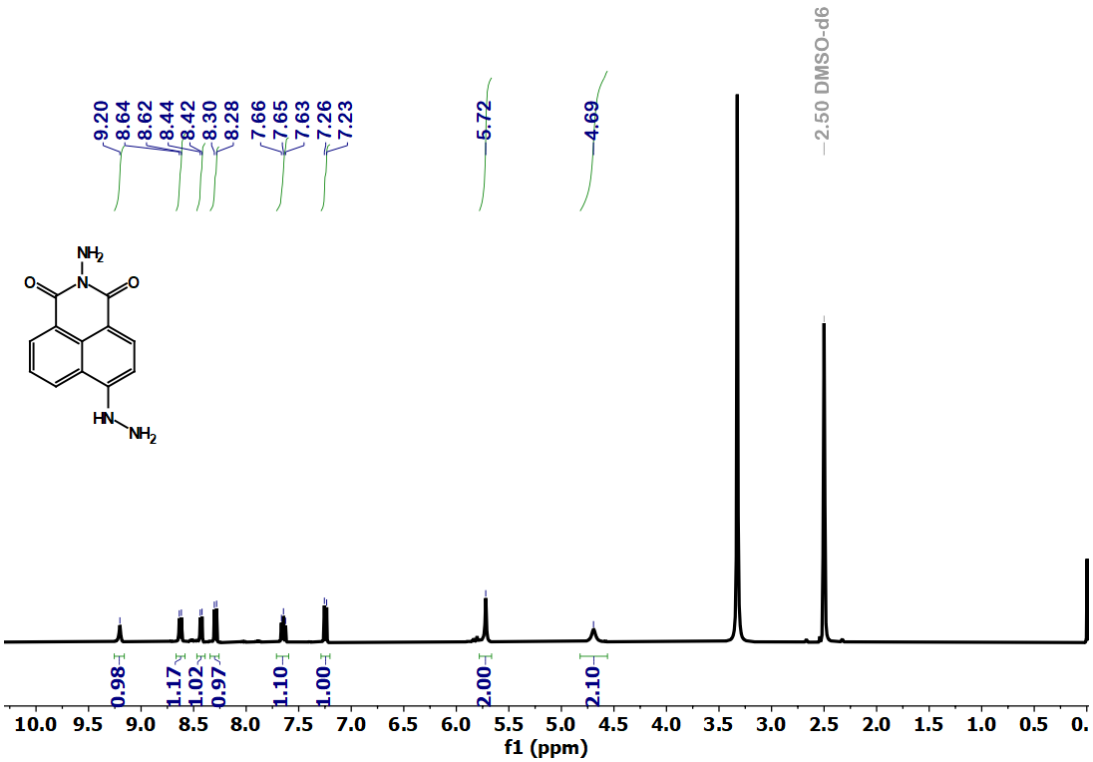

Figure S57. ^{1}H NMR spectrum of ligand after treatement of NH_2NH_2.

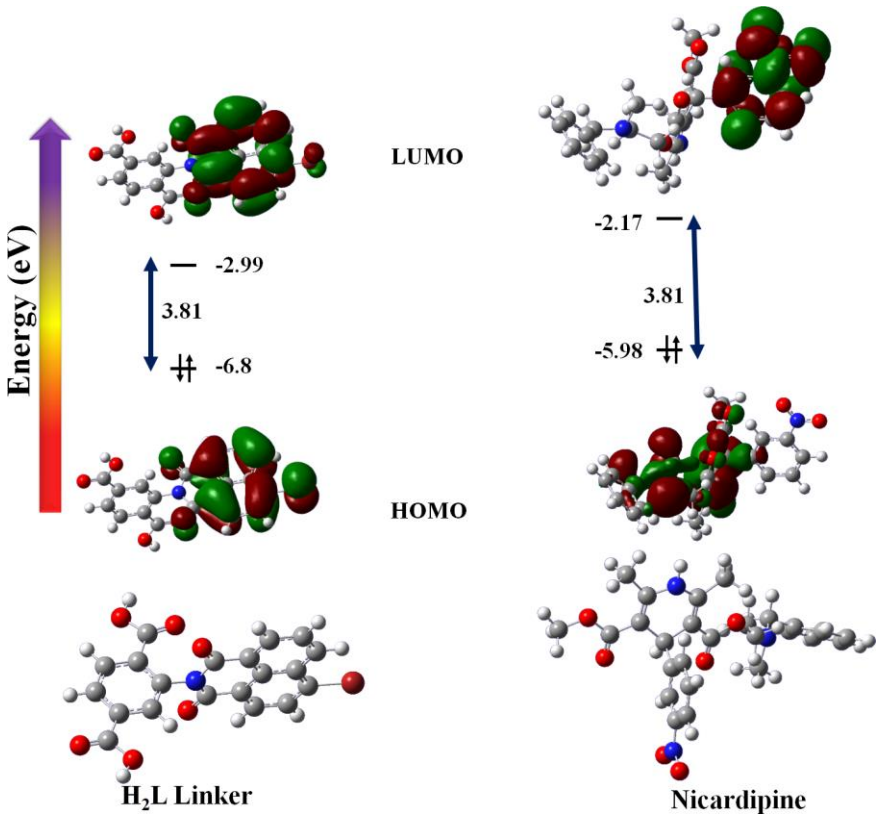

Figure S58. HOMO and LUMO energy levels of the free linker of MOF and nicardipine.

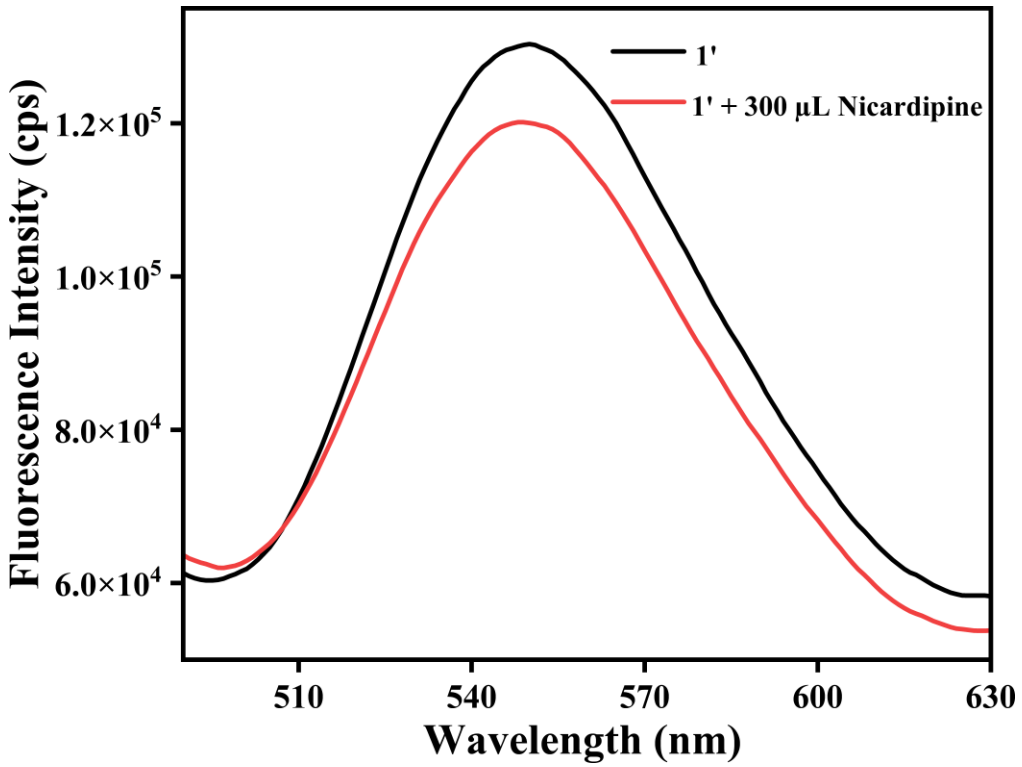

Figure S59. Change of fluorescence intensity of the probe **1'** in presence of nicardipine when the probe was excited at 400 nm.

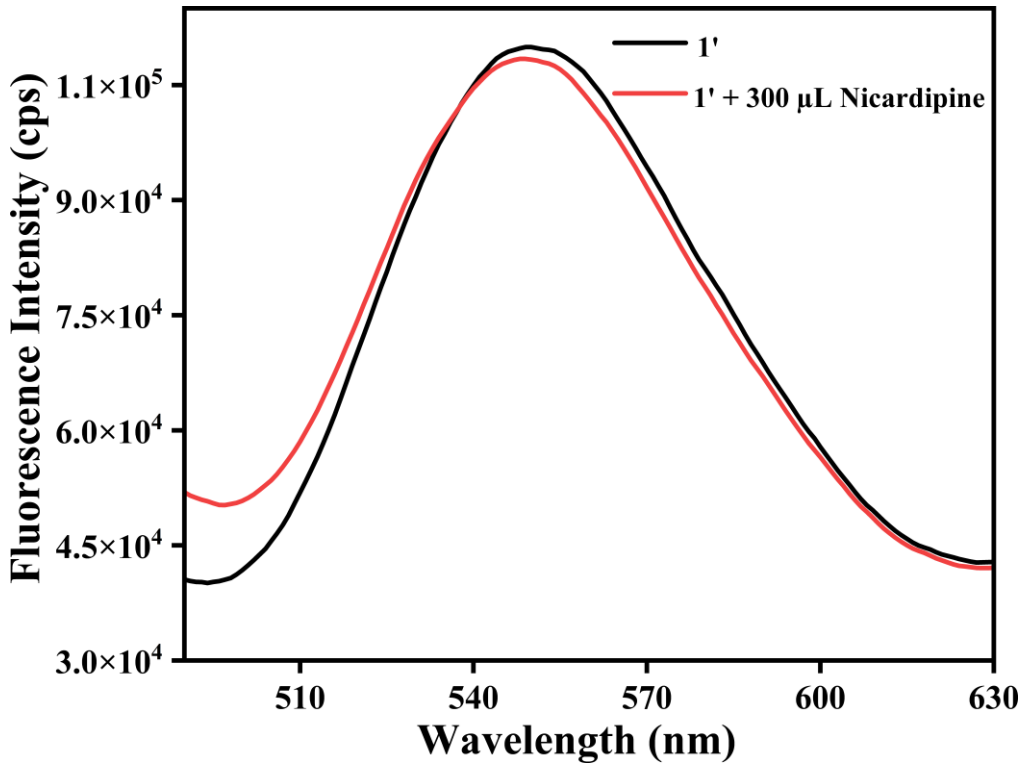

Figure S60. Change of fluorescence intensity of the probe **1'** in presence of nicardipine when the probe was excited at 450 nm.

Table S3. Comparison of the response time, detection limit and analyte used for the reported chemosensors of NH_2NH_2 in the literature.

Sl. No.	Sensor Material	Type of Material	Sensing Medium	Mode of Detection	Detection Limit	Response Time	Ref
1	**$[Zr_6O_4(OH)_4(C_{20}H_8BrNO_6)_3(C_2O_2F_3)_6]\cdot 7H_2O \cdot 2.5DMF$**	**MOF**	**water**	**turn-on**	**1.11 nM**	**100 s**	**this work**
2	Zr-UiO-66-$(OCOCH_3)_2$	MOF	water	turn-on	78.8 nM	-	2
7	Naphsulf-O	organic-molecule	PBS buffer	turn-on	22 nM	40 min	3
8	BBHC	organic-molecule	PBS buffer	turn-on	0.43 µM	1 min	4
9	UiO-66-phmd	MOF	HEPES buffer	turn-on	0.87 µM	20 min	5
10	BI-E	near-infrared fluorescent probe	PBS buffer	turn-on	0.057 µM	1 min	6

11	NA-N_2H_4	naphthalimide based organic molecule	HEPES buffer	ratio-metric	9.4 nM	15 min	7
12	TAPHP	organic-molecule	HEPES buffer	ratio-metric	0.3 μM	60 min	8
13	HBTM	organic-molecule	PBS buffer	turn-on	29 μM	55 min	9
14	NAC	naphthalene based organic molecule	HEPES buffer	turn-on	4.5 μM	4 min	10
17	DPA	organic-molecule	DMSO/ PBS buffer solution (4/6, v/v)	turn-on	1.9 nM	8 min	11
19	levulinated hydroxyl-coumarin 1	organic-molecule	acetate buffer	turn-on	2.46 μM	15 min	12
24	PBF	organic-molecule	CH_3CN–H_2O (6: 4, v/v)	turn-on	0.41 μM	1 min	13

Simulated Crystallographic Information File (CIF) for Guest-Free Compound 1.

data_Compound 1

_audit_creation_date 2024-03-05

_audit_creation_method 'Materials Studio'

_symmetry_space_group_name_H-M 'R3'

_symmetry_Int_Tables_number 146

_symmetry_cell_setting trigonal

loop_

_symmetry_equiv_pos_as_xyz

x,y,z

-y,x-y,z

-x+y,-x,z

x+2/3,y+1/3,z+1/3

-y+2/3,x-y+1/3,z+1/3

-x+y+2/3,-x+1/3,z+1/3

x+1/3,y+2/3,z+2/3

-y+1/3,x-y+2/3,z+2/3

-x+y+1/3,-x+2/3,z+2/3

_cell_length_a 14.6530

_cell_length_b 14.6530

_cell_length_c 35.9120

_cell_angle_alpha 90.0000

_cell_angle_beta 90.0000

_cell_angle_gamma 120.0000

loop_

_atom_site_label

_atom_site_type_symbol

_atom_site_fract_x

_atom_site_fract_y

_atom_site_fract_z

_atom_site_U_iso_or_equiv

_atom_site_adp_type

_atom_site_occupancy

Zr1	Zr	0.07521	0.14930	0.02338	0.05000	Uiso	1.00
Zr2	Zr	0.58947	0.40622	0.27944	0.05000	Uiso	1.00
O3	O	0.17282	0.15718	0.06884	0.05000	Uiso	1.00
O4	O	0.04686	0.27292	0.01421	0.05000	Uiso	1.00
O5	O	0.49871	0.32206	0.23155	0.05000	Uiso	1.00
O6	O	0.50330	0.16717	0.23107	0.05000	Uiso	1.00
O7	O	0.17431	0.00197	0.06935	0.05000	Uiso	1.00
O8	O	0.15403	0.07740	0.00388	0.05000	Uiso	1.00
O9	O	0.07567	0.15476	0.96541	0.05000	Uiso	1.00
O10	O	0.22660	0.27461	0.01237	0.05000	Uiso	1.00
O11	O	0.43993	0.38418	0.29169	0.05000	Uiso	1.00
O12	O	0.60735	0.55291	0.29527	0.05000	Uiso	1.00

N13	N	0.20933	0.24949	0.13798	0.05000	Uiso	1.00
C14	C	0.27689	0.20531	0.14206	0.05000	Uiso	1.00
C15	C	0.34195	0.23536	0.17400	0.05000	Uiso	1.00
C16	C	0.41543	0.12956	0.15475	0.05000	Uiso	1.00
C17	C	0.35011	0.09798	0.12260	0.05000	Uiso	1.00
C18	C	0.20413	0.09513	0.08248	0.05000	Uiso	1.00
C19	C	0.27780	0.13347	0.11587	0.05000	Uiso	1.00
C20	C	0.47579	0.23136	0.21677	0.05000	Uiso	1.00
C21	C	0.41089	0.19798	0.18136	0.05000	Uiso	1.00
H22	H	0.33597	0.28696	0.19401	0.06000	Uiso	1.00
H23	H	0.46984	0.10074	0.15869	0.06000	Uiso	1.00
H24	H	0.35644	0.04565	0.10285	0.06000	Uiso	1.00
C25	C	0.62727	0.67691	0.65591	0.00000	Uiso	1.00
C26	C	0.66370	0.04083	0.31928	0.00000	Uiso	1.00
C27	C	0.73023	0.68303	0.65800	0.00000	Uiso	1.00
C28	C	0.66093	0.93936	0.32115	0.00000	Uiso	1.00
H29	H	0.45036	0.55559	0.62273	0.00000	Uiso	1.00
F30	F	0.72976	0.61406	0.63189	0.00000	Uiso	1.00
F31	F	0.74528	0.65376	0.69309	0.00000	Uiso	1.00
F32	F	0.80944	0.78497	0.65065	0.00000	Uiso	1.00
F33	F	0.86264	0.57054	0.65929	0.00000	Uiso	1.00
F34	F	0.93117	0.71464	0.62198	0.00000	Uiso	1.00
F35	F	0.95059	0.73404	0.68449	0.00000	Uiso	1.00
C36	C	0.56677	0.99481	0.77875	0.00000	Uiso	1.00
C37	C	0.51702	0.06055	0.78148	0.00000	Uiso	1.00
C38	C	0.47484	0.06458	0.81601	0.00000	Uiso	1.00
C39	C	0.45211	0.98592	0.84256	0.00000	Uiso	1.00
C40	C	0.47447	0.90128	0.83341	0.00000	Uiso	1.00
O41	O	0.77331	0.48950	0.51971	0.00000	Uiso	1.00
O42	O	0.96868	0.68292	0.42210	0.00000	Uiso	1.00

C43 C 0.18322 0.97672 0.49128 0.00000 Uiso 1.00

C44 C 0.11320 0.91762 0.46287 0.00000 Uiso 1.00

C45 C 0.12575 0.95880 0.42690 0.00000 Uiso 1.00

C46 C 0.20359 0.06249 0.41970 0.00000 Uiso 1.00

C47 C 0.33732 0.09207 0.54502 0.00000 Uiso 1.00

C48 C 0.24626 -0.00066 0.55478 0.00000 Uiso 1.00

C49 C 0.16944 0.94084 0.52830 0.00000 Uiso 1.00

Br50 Br 0.51232 0.88866 0.21216 0.00000 Uiso 1.00

H51 H 0.78867 0.94929 0.46849 0.00000 Uiso 1.00

H52 H 0.83862 0.92682 0.40481 0.00000 Uiso 1.00

H53 H 0.88775 0.79178 0.39241 0.00000 Uiso 1.00

H54 H 0.74012 0.60389 0.56587 0.00000 Uiso 1.00

H55 H 0.74166 0.76697 0.58327 0.00000 Uiso 1.00

O56 O 0.00000 0.00000 0.04492 0.05000 Uiso 1.00

O57 O 0.66667 0.33333 0.25843 0.05000 Uiso 1.00

H58 H 0.66667 0.33333 0.40582 0.00000 Uiso 1.00

loop_

_geom_bond_atom_site_label_1

_geom_bond_atom_site_label_2

_geom_bond_distance

_geom_bond_site_symmetry_2

_ccdc_geom_bond_type

Zr1 O3 2.135 . S

Zr1 O4 2.077 . S

Zr1 O8 2.038 . S

Zr1 O9 2.083 1_554 S

Zr1 O10 2.092 . S

Zr1 O56 2.047 . S

Zr1 O7 2.121 2 S

Zr1 O8 2.060 2 S

Zr2	O5	2.147	.	S
Zr2	O11	2.095	.	S
Zr2	O12	2.109	.	S
Zr2	O57	2.049	.	S
Zr2	O6	2.126	3_665	S
Zr2	O9	2.061	4_554	S
Zr2	O8	2.075	5	S
Zr2	O9	2.050	5_554	S
O3	C18	1.301	.	A
O4	C25	1.289	5_554	A
O5	C20	1.309	.	A
O6	C20	1.300	.	A
O6	Zr2	2.126	2_655	S
O7	C18	1.296	.	A
O7	Zr1	2.121	3	S
O8	Zr1	2.060	3	S
O8	Zr2	2.075	9_554	S
O9	Zr1	2.083	1_556	S
O9	Zr2	2.061	7_445	S
O9	Zr2	2.050	9	S
O9	H29	0.989	5	S
O10	C26	1.292	8_544	A
O11	C26	1.294	3_665	A
O12	C25	1.298	8_654	A
N13	C14	1.436	.	S
N13	C36	1.382	4_444	S
N13	C40	1.377	4_444	S
C14	C15	1.414	.	A
C14	C19	1.417	.	A
C15	C21	1.394	.	A

C15 H22 1.078 . S

C16 C17 1.421 . A

C16 C21 1.410 . A

C16 H23 1.082 . S

C17 C19 1.415 . A

C17 H24 1.082 . S

C18 C19 1.521 . S

C20 C21 1.515 . S

C25 O4 1.289 9 A

C25 O12 1.298 6_565 A

C25 C27 1.468 . S

C26 O11 1.294 2_655 A

C26 O10 1.292 6 A

C26 C28 1.469 1_545 S

C27 F30 1.376 . S

C27 F31 1.384 . S

C27 F32 1.384 . S

C28 C26 1.469 1_565 S

C28 F33 1.384 8_654 S

C28 F34 1.383 8_654 S

C28 F35 1.382 8_654 S

H29 O9 0.989 9_554 S

F33 C28 1.384 6_565 S

F34 C28 1.383 6_565 S

F35 C28 1.382 6_565 S

C36 C37 1.474 1_565 S

C36 N13 1.382 7 S

C36 O42 1.222 4_455 D

C37 C36 1.474 1_545 S

C37 C38 1.400 . A

C37	C46	1.400	6	A
C38	C39	1.402	1_545	A
C38	C43	1.408	6_455	A
C39	C38	1.402	1_565	A
C39	C40	1.470	.	S
C39	C47	1.394	6_565	A
C40	N13	1.377	7	S
C40	O41	1.222	4_455	D
O41	C40	1.222	7_544	D
O42	C36	1.222	7_544	D
C43	C44	1.398	.	A
C43	C38	1.408	8_554	A
C43	C49	1.407	.	A
C44	C45	1.398	.	A
C44	H51	1.069	2_665	S
C45	C46	1.394	1_565	A
C45	H52	1.080	2_665	S
C46	C45	1.394	1_545	A
C46	C37	1.400	8_544	A
C46	H53	1.083	2_655	S
C47	C48	1.392	.	A
C47	C39	1.394	8_654	A
C47	H54	1.079	2_655	S
C48	C49	1.393	1_545	A
C48	H55	1.070	2_655	S
C49	C48	1.393	1_565	A
C49	Br50	1.909	6_465	S
Br50	C49	1.909	8_664	S
H51	C44	1.069	3_565	S
H52	C45	1.080	3_565	S

H53 C46 1.083 3_665 S

H54 C47 1.079 3_665 S

H55 C48 1.070 3_665 S

O56 Zr1 2.047 2 S

O56 Zr1 2.047 3 S

O56 H58 0.990 7_444 S

O57 Zr2 2.049 2_655 S

O57 Zr2 2.049 3_665 S

H58 O56 0.990 4 S

References:

(1) Farha, O. K.; Özgür Yazaydın, A.; Eryazici, I.; Malliakas, C. D.; Hauser, B. G.; Kanatzidis, M. G.; Nguyen, S. T.; Snurr, R. Q.; Hupp, J. T. De novo synthesis of a metal–organic framework material featuring ultrahigh surface area and gas storage capacities. *Nat. Chem.* **2010**, *2* (11), 944-948.

(2) Nandi, S.; Mostakim, S.; Biswas, S. Rapid switch-on fluorescent detection of nanomolar-level hydrazine in water by a diacetoxy-functionalized MOF: application in paper strips and environmental samples. *Dalton Trans.* **2020**, *49* (36), 12565-12573.

(3) Mahapatra, A. K.; Maji, R.; Maiti, K.; Manna, S. K.; Mondal, S.; Ali, S. S.; Manna, S.; Sahoo, P.; Mandal, S.; Uddin, M. R. A BODIPY/pyrene-based chemodosimetric fluorescent chemosensor for selective sensing of hydrazine in the gas and aqueous solution state and its imaging in living cells. *RSC Adv.* **2015**, *5* (72), 58228-58236.

(4) Chen, W.; Liu, W.; Liu, X.-J.; Kuang, Y.-Q.; Yu, R.-Q.; Jiang, J.-H. A novel fluorescent probe for sensitive detection and imaging of hydrazine in living cells. *Talanta* **2017**, *162*, 225-231.

(5) Mostakim, S.; Khan, M. R. U. Z.; Das, A.; Nandi, S.; Trivedi, V.; Biswas, S. A phthalimide-functionalized UiO-66 metal–organic framework for the fluorogenic detection of hydrazine in live cells. *Dalton Trans.* **2019**, *48* (33), 12615-12621.

(6) Zhang, Z.; Zhuang, Z.; Song, L.; Zhang, S.; Zheng, G.; Zhan, F. A FRET-based ratiometric fluorescent probe for hydrazine and its application in living cells. *J. Photochem. Photobiol.* **2018**, *358*, 10-16.

(7) Ma, J.; Fan, J.; Li, H.; Yao, Q.; Xia, J.; Wang, J.; Peng, X. Probing hydrazine with a near-infrared fluorescent chemodosimeter. *Dyes Pigments* **2017**, *138*, 39-46.

(8) Xia, X.; Zeng, F.; Zhang, P.; Lyu, J.; Huang, Y.; Wu, S. An ICT-based ratiometric fluorescent probe for hydrazine detection and its application in living cells and in vivo. *Sens. Actuators B: Chem.* **2016**, *227*, 411-418.

(9) Luo, Z.; Liu, B.; Qin, T.; Zhu, K.; Zhao, C.; Pan, C.; Wang, L. Cyclization of chalcone enables ratiometric fluorescence determination of hydrazine with a high selectivity. *Sens. Actuators B: Chem.* **2018**, *263*, 229-236.

(10) Zhou, D.; Wang, Y.; Jia, J.; Yu, W.; Qu, B.; Li, X.; Sun, X. H-Bonding and charging mediated aggregation and emission for fluorescence turn-on detection of hydrazine hydrate. *Chem. Commun.* **2015**, *51* (53), 10656-10659.

(11) Goswami, S.; Das, A. K.; Saha, U.; Maity, S.; Khanra, K.; Bhattacharyya, N. Rapid detection of hydrazine in a naphthol-fused chromenyl loop and its effectiveness in human lung cancer cells: tuning remarkable selectivity via the reaction altered pathway supported by theoretical studies. *Org. Biomol. Chem.* **2015**, *13* (7), 2134-2139.
(12) Roy, B.; Halder, S.; Guha, A.; Bandyopadhyay, S. Highly selective sub-ppm naked-eye detection of hydrazine with conjugated-1, 3-diketo probes: imaging hydrazine in drosophila larvae. *Anal. Chem.* **2017**, *89* (19), 10625-10636.
(13) Goswami, S.; Paul, S.; Manna, A. Fast and ratiometric "naked eye" detection of hydrazine for both solid and vapour phase sensing. *New J. Chem.* **2015**, *39* (3), 2300-2305.